Earth's Future

RESEARCH ARTICLE
10.1029/2023EF004358

Identifying Climate Impacts From Different Stratospheric Aerosol Injection Strategies in UKESM1

Alice F. Wells[1], Matthew Henry[1], Ewa M. Bednarz[2,3,4], Douglas G. MacMartin[4], Andy Jones[5], Mohit Dalvi[5], and James M. Haywood[1,5]

[1]Faculty of Environment, Science and Economy, Department of Mathematics and Statistics, University of Exeter, Exeter, UK, [2]Cooperative Institute for Research in Environmental Sciences (CIRES), University of Colorado Boulder, Boulder, CO, USA, [3]NOAA Chemical Sciences Laboratory (NOAA CSL), Boulder, CO, USA, [4]Sibley School of Mechanical and Aerospace Engineering, Cornell University, Ithaca, NY, USA, [5]Met Office, Exeter, UK

Abstract Stratospheric Aerosol Injection (SAI) is a proposed method of climate intervention aiming to reduce the impacts of human-induced global warming by reflecting a portion of incoming solar radiation. Many studies have demonstrated that SAI would successfully reduce global-mean surface air temperatures; however the vast array of model scenarios and strategies result in a diverse range of climate impacts. Here we compare two SAI strategies—a quasi- equatorial injection and a multi-latitude off-equatorial injection—simulated with the UK Earth System Model (UKESM1), both aiming to reduce the global-mean surface temperature from that of a high-end emissions scenario to that of a moderate emissions scenario. We compare changes in the surface and stratospheric climate under each strategy to determine how the climate response depends on the injection location. In agreement with previous studies, an equatorial injection results in a tropospheric overcooling in the tropics and a residual warming in the polar regions, with substantial changes to stratospheric temperatures, water vapor and circulation. Previous comparisons of equatorial versus off-equatorial injection strategies are limited to two studies using different versions of the Community Earth System Model. Our study evaluates how the climate responds in UKESM1 under these injection strategies. Our results are broadly consistent with previous findings, concluding that an off-equatorial injection strategy can minimize regional surface temperature and precipitation changes relative to the target. We also present more in-depth analysis of the associated changes in Hadley Circulation and regional temperature changes, and call for a new series of inter-model SAI comparisons using an off-equatorial strategy.

Plain Language Summary Stratospheric Aerosol Injection (SAI) is a method to tackle the impacts of global warming and involves reflecting some of the sun's rays away from Earth. Different strategies for implementing SAI can have various effects on the climate. This study compares two strategies—one injecting at the equator and the other at different latitudes. Both strategies successfully lower global temperatures, but they also lead to different regional climate changes. The equatorial strategy cools the tropics too much and doesn't cool the poles enough. Whereas the off-equatorial strategy minimizes some of the negative impacts seen in the equatorial strategy. In summary, injecting aerosols away from the equator avoids unfavorable climate impacts.

Key Points:

- We compare the climate impacts of equatorial and multi-latitude Stratospheric Aerosol Injection (SAI) strategies under the Geoengineering Model Intercomparison Project G6 framework
- We demonstrate that an off-equatorial multi-latitude injection strategy minimizes unfavorable climate impacts
- This research highlights the importance of injection location in determining the impacts of SAI on the climate

Supporting Information:

Supporting Information may be found in the online version of this article.

Correspondence to:

A. F. Wells,
a.wells@exeter.ac.uk

Citation:

Wells, A. F., Henry, M., Bednarz, E. M., MacMartin, D. G., Jones, A., Dalvi, M., & Haywood, J. M. (2024). Identifying climate impacts from different stratospheric aerosol injection strategies in UKESM1. *Earth's Future*, *12*, e2023EF004358. https://doi.org/10.1029/2023EF004358

Received 8 DEC 2023
Accepted 6 MAR 2024

Author Contributions:

Conceptualization: Alice F. Wells, James M. Haywood
Data curation: Andy Jones, Mohit Dalvi
Formal analysis: Alice F. Wells
Funding acquisition: James M. Haywood
Methodology: Alice F. Wells, Ewa M. Bednarz, Andy Jones, James M. Haywood
Supervision: Matthew Henry, Ewa M. Bednarz, Douglas G. MacMartin, Andy Jones, James M. Haywood
Visualization: Alice F. Wells
Writing – original draft: Alice F. Wells
Writing – review & editing: Alice F. Wells, Matthew Henry, Ewa

1. Introduction

The climate is warming at an unprecedented rate with global mean temperatures projected to reach or exceed the 1.5°C Paris agreement temperature goal within the next 20 years (Masson-Delmotte et al., 2021). Increases in the number of extreme weather events have already been observed in recent years including extreme precipitation events, droughts, and heatwaves. Under global warming, the frequency and intensity of such events are projected to increase (Seneviratne et al., 2021). Mitigation efforts have been made with net-zero pledges reducing projected 2030 global emissions by 7.5% (UNEP, 2021), however due to the long lifetime of CO_2 the impacts of climate change are likely to continue. These factors have resulted in an increasing interest in climate intervention strategies.

Solar climate intervention (SCI), otherwise known as solar radiation modification (SRM), methods aim to increase the planetary albedo and induce a surface cooling, thereby reducing some of the undesirable impacts of global warming on the weather and climate. These proposed techniques aim to reduce increasing temperatures whilst mitigation efforts continue and greenhouse gases (GHGs) are removed from the atmosphere. Recently,

support for SRM research has grown with two reports advocating for more robust scientific research. The US National Academies of Sciences, Engineering and Medicine (NASEM) report on solar geoengineering research and research governance (NASEM, 2021) proposed a $200 million investment into a research program to better understand the risks, benefits and impacts of SCI strategies. The United Nations Environment Programme (UNEP) also called for robust, equitable and rigorous trans-disciplinary research to reduce uncertainties associated with SRM (UNEP, 2023).

One of the proposed methods of SRM, Stratospheric Aerosol Injection (SAI), originally proposed by Budyko (1977) and revisited by Crutzen (2006), aims to mimic the effect of a large volcanic eruption by injecting SO_2 into the stratosphere to produce a layer of sulfate aerosols which can reflect a small portion of the incoming solar radiation. Whilst there are some differences between a single pulse injection of SO_2 from a volcanic eruption and the continual injection needed to consistently cool the planet (MacMartin et al., 2016; Robock et al., 2013), volcanic eruptions act as natural analogs for assessing the capability of global climate models to model SAI (e.g., Trenberth & Dai, 2007). Model uncertainties (Bednarz et al., 2023c; Henry et al., 2023; Niemeier & Timmreck, 2015; Visioni et al., 2021, 2023a) and different SAI scenario choices, including the choice of baseline emissions scenario (Fasullo & Richter, 2023), injection location or strategy (Bednarz et al., 2023a; Franke et al., 2021; Heckendorn et al., 2009; Kravitz et al., 2019; Zhang et al., 2024), temperature target (Bednarz et al., 2023b; Hueholt et al., 2023; MacMartin et al., 2022; Visioni et al., 2023b) and timing of SAI deployment (Brody et al., 2024) can result in different large-scale climate responses and the associated regional impacts.

To assess model uncertainties, similar experiments can be compared across different models. This is a common approach in climate modeling, with the results from multiple models forced by nominally identical shared socioeconomic pathway GHG emission scenarios being frequently used in the climate change context (e.g., Masson-Delmotte et al., 2021). Similarly, inconsistent SRM results between multiple models (e.g., A. Jones et al., 2010; Rasch et al., 2008) motivated the Geoengineering Model Intercomparison Project (GeoMIP) as a means to help untangle those differences by creating a set of standardized experiments. The latest GeoMIP experiments, which align with the latest CMIP6 scenarios, include G6solar and G6sulfur (Kravitz et al., 2013, 2015). The aim of these experiments was to reduce global mean surface air temperatures under the otherwise high-end SSP5-8.5 emissions scenario to those of the more moderate SSP2-4.5 (O'Neill et al., 2016). This was achieved by either reducing the solar constant (G6solar) or by injecting SO_2 between 10°N and 10°S and between 18 and 20 km (G6sulfur). Very recent simulations that cool the climate from the SSP5-8.5 scenario to that of SSP2-4.5 using explicit injections of sea-salt within the UKESM1 climate model have also been performed (G6MCB; Haywood et al., 2023).

Outside of GeoMIP, experiments using the Community Earth System Model (CESM) and UKESM1 have been performed using control theory to modify the annual injection of SO_2 across multiple locations (MacMartin & Kravitz, 2019). Studies include the Geoengineering Large ENSemble (GLENS) project (GLENS; Tilmes et al., 2018a) and the Assessing Responses and Impacts of SCI of the Earth system with SAI project (ARISE-SAI; Richter et al., 2022). These experiments injected SO_2 at multiple latitudes (30°S, 15°S, 15°N, 30°N) away from the equator and controlled not only the global-mean surface air temperature, but also its interhemispheric and equator-to-pole temperature gradients (Kravitz et al., 2017; MacMartin et al., 2017). The motivation behind the inclusion of the latter two temperature targets under a feedback controller were to reduce the tropical overcooling and polar undercooling simulated under many equatorial injections (Kravitz et al., 2016) whilst also minimizing any changes to the position of the InterTropical Convergence Zone (ITCZ) and the associated precipitation patterns (Haywood et al., 2013). Under the GLENS SAI scenario framework, Kravitz et al. (2019) demonstrated that using a multi-latitude off-equatorial injection strategy in CESM1 can minimize the residual impacts on regional surface air temperature and precipitation when compared to the same scenario using an equatorial injection strategy. In that case, temperatures were held constant with SAI at 2020 levels under the high-end RCP8.5 warming scenario, requiring large injections of SO_2 by the end of the century.

Here, we pursue a methodology similar to that in Kravitz et al. (2019); we compare the global climate response to a quasi-equatorial injection strategy, G6sulfur, and an equivalent off-equatorial multi-latitude injection strategy, G6controller. G6controller uses the feedback controller (Kravitz et al., 2017; MacMartin & Kravitz, 2019; MacMartin et al., 2018) to meet the yearly global mean surface air temperature of SSP2-4.5 as in the G6sulfur scenario design. It is also designed to meet the interhemispheric and equator-to-pole temperature gradients similar

to GLENS and ARISE. By making the comparison between G6sulfur and G6controller we can determine if the results seen in Kravitz et al. (2019), comparing GLENS to an equatorial injection, are consistent with those from UKESM1 and under the GeoMIP framework. After describing the model and the scenario and strategy design in Section 2 we compare the injection rate of each strategy and their ability to meet the desired temperature targets (Section 3). We then compare the surface air temperature (Section 4) and precipitation response (Section 5.1) under each strategy before we analyze the stratospheric response in Section 6.

2. Methods

Previous studies have documented the GeoMIP G6sulfur simulations and the UKESM1 model (e.g., Haywood et al., 2022; A. Jones et al., 2020), so only a brief summary of the G6sulfur simulations and the model are provided here. Similarly, the implementation of the controller (Kravitz et al., 2017; MacMartin & Kravitz, 2019) within the UKESM1 model is described in Henry et al. (2023).

2.1. Model Description

UKESM1, the latest UK Earth system model, is described by Sellar et al. (2019). It consists of the HadGEM3 coupled physical climate model with a resolution of 1.25° latitude by 1.875° longitude with 85 vertical levels and a model top at approximately 85 km. This is coupled to a 1° resolution ocean model with 75 levels (Storkey et al., 2018). It includes additional interactive components to model tropospheric and stratospheric chemistry (Archibald et al., 2020), ocean biogeochemistry (Yool et al., 2013), sea ice (Ridley et al., 2018), land surface and vegetation (Best et al., 2011) and aerosols (Mann et al., 2010). The merged stratospheric and tropospheric scheme, StratTrop as described by Archibald et al. (2020), simulates interactive chemistry from the surface to the top of the model which includes the oxidation reactions responsible for sulfate aerosol production (Sellar et al., 2019). Evaluation of the evolution of stratospheric aerosols from explosive volcanic eruptions in UKESM1 have been performed and the model shows reasonable fidelity (e.g., Dhomse et al., 2020; Wells, Jones, Osborne, et al., 2023).

Atmospheric composition in UKESM1 is simulated by the UK Chemistry and Aerosols (UKCA) sub-model. The GLOMAP-mode modal aerosol scheme, as described in Mann et al. (2010, 2012), is a two-moment aerosol microphysics scheme and is one of the main components of UKCA. It simulates speciated aerosol mass and number across five lognormal size modes, four soluble modes—nucleation, Aitken, accumulation and coarse modes, and one insoluble Aitken mode.

2.2. Simulation Set Up/Design and Analysis Framework

This study analyses four sets of simulations, with three ensemble members for each, from 2020 to 2100. These include two baseline scenarios which follow the Shared Socioeconomic Pathways SSP2-4.5 and SSP5-8.5 as described by O'Neill et al. (2016), and two SAI strategies, G6sulfur (first presented in A. Jones et al. (2020)) and G6controller (presented here for the first time). As described in Kravitz et al. (2015), the aim of G6sulfur is to modify high-end emission scenario SSP5-8.5 simulations so that the global mean surface air temperature is reduced to that of the moderate emissions scenario SSP2-4.5. In the UKESM1 G6sulfur simulations, the SSP5-8.5 decadal-mean global mean surface air temperature is reduced to within 0.2 K of the corresponding SSP2-4.5 temperature through manually adjusting the magnitude of SO_2 injection into the lower stratosphere (A. Jones et al., 2020). In particular, the injection is applied uniformly between 10°N and 10°S along the Greenwich meridian at 18–20 km, with the amount of SO_2 adjusted every 10 years to meet SSP2-4.5 targets.

Whilst G6controller follows the same overarching scenario as G6sulfur, reducing global mean surface air temperature from SSP5-8.5 to SSP2-4.5, the injection strategy is more complex. Similarly to the GLENS (Tilmes et al., 2018a) and the ARISE-SAI (Richter et al., 2022) strategies, G6controller injects SO_2 at four latitudes—30°N, 15°N, 15°S and 30°S—and a slightly higher altitude of 21.5 km using a feedback algorithm (as described by Henry et al. (2023), Kravitz et al. (2017), and MacMartin et al. (2018)) that adjusts the injection rate at each location to meet simultaneous temperature targets, namely: the global mean surface air temperature (T_0), the interhemispheric surface air temperature gradient (T_1), and the equator-to-pole surface air temperature gradient (T_2). T_1 and T_2 are defined in Equation 1 from Kravitz et al. (2017). One subtle difference between the implementation of the controller in these simulations and the previous works (e.g., Henry et al., 2023; Kravitz et al., 2019; Richter et al., 2022; Tilmes et al., 2018a) is that, rather than fixed targets, T_0, T_1 and T_2 are transient

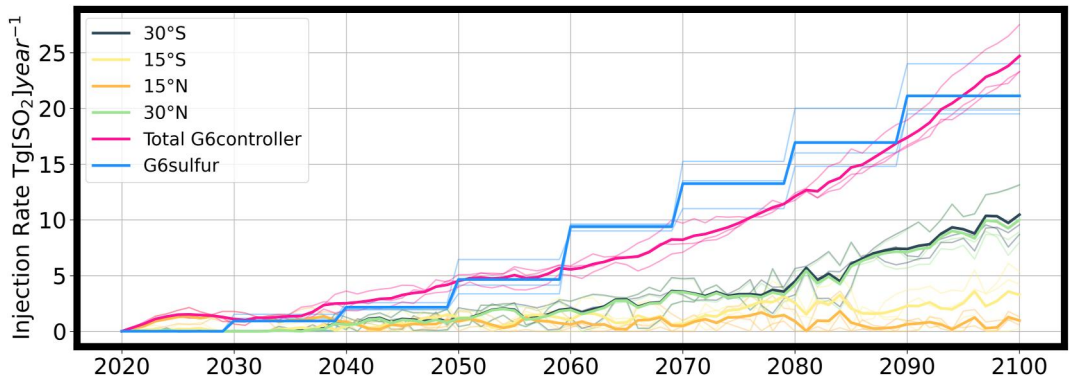

Figure 1. Annual injection rates (Tg[SO_2] $year^{-1}$) for G6sulfur (blue) and G6controller (pink), with the injections at each individual latitude in G6controller shown in other colors. The thick lines represent the ensemble mean, whereas thin lines show each ensemble member.

values determined from the SSP2-4.5 simulations. Each year the targets are calculated from each SSP2-4.5 ensemble member resulting in the adjustment of the amount and location of SO_2 injected in the corresponding G6controller ensemble member.

While many of the results that are presented here show either the global or zonal mean responses, in Section 4 we also present results of regional surface air temperature changes by calculating regional means over the 46 land-only reference regions (Iturbide et al., 2020) produced for the Intergovernmental Panel on Climate Change Assessment Report 6 (Masson-Delmotte et al., 2021). These areas (henceforth AR6) are shown in Figure S1 in Supporting Information S1 with abbreviations for region names, colored by continent.

3. Large Scale Temperature Targets and SO_2 Injections

The SO_2 injection rate in both strategies is comparable throughout the 80 years of the simulations (Figure 1). Cumulatively G6sulfur injects around 10% more than G6controller (705 Tg compared to 645 Tg) to reach roughly the same global mean surface temperatures (Figure 2a). The lower efficiency of G6sulfur compared to G6controller is at least in part driven by the differences in the injection altitudes, 21.5 km for G6controller and 18–20 km for G6sulfur; a lower injection altitude reduces lifetime of sulfate aerosols and, thus, the overall efficiency. Studies with the CESM model have also shown that equatorial injections can be less efficient at offsetting global mean temperatures than off-equatorial strategies (e.g., Kravitz et al., 2019; Zhang et al., 2024). There are also studies which show a greater efficiency and temperature change from a radiative forcing applied at higher latitudes relative to one applied at the equator (e.g., Zhao et al., 2021). In this case, it is likely a combination of effects, however the difference in injection altitude is likely the dominant cause of the difference in efficiency as simulations with a predecessor of UKESM1 model have shown that the radiative forcing and temperature change are strong functions of altitude, and more weakly dependent on the latitude of the injection (A. C. Jones et al., 2016, 2017).

For G6controller, the majority of the SO_2 is injected at 30°N and 30°S from 2040 onwards and by the end of century only 20% of the total SO_2 is injected at 15°N and 15°S. This is generally similar to the UKESM1 ARISE-SAI-1.5 simulations described in Henry et al. (2023), where most of the injection also occurs at the subtropical latitudes (i.e., 30°N and 30°S). However, a notable difference is that G6controller continues to mostly inject at these two latitudes throughout the simulation while Henry et al. (2023) report a marked increase in injection at 15°N halfway through their simulation. This is likely partly due to the differences in the underlying scenarios (i.e., SSP5-8.5 here vs. SSP2-4.5 in ARISE-SAI-1.5) which have been found to be important in other SAI simulations (Fasullo & Richter, 2023). The similarity of the large-scale UKESM1 temperature responses to injections at 15°N and 30°N determined from the 10-year long sensitivity runs used to train the controller (Visioni et al., 2023a) can lead to relatively large changes in the controller's partitioning of injections over these latitudes under comparatively small changes in the underlying climate.

Figure 2 shows how each strategy performs over the 80 years of the simulations with respect to the three temperature targets; global mean surface air temperature (T_0), the interhemispheric temperature gradient (T_1) and the

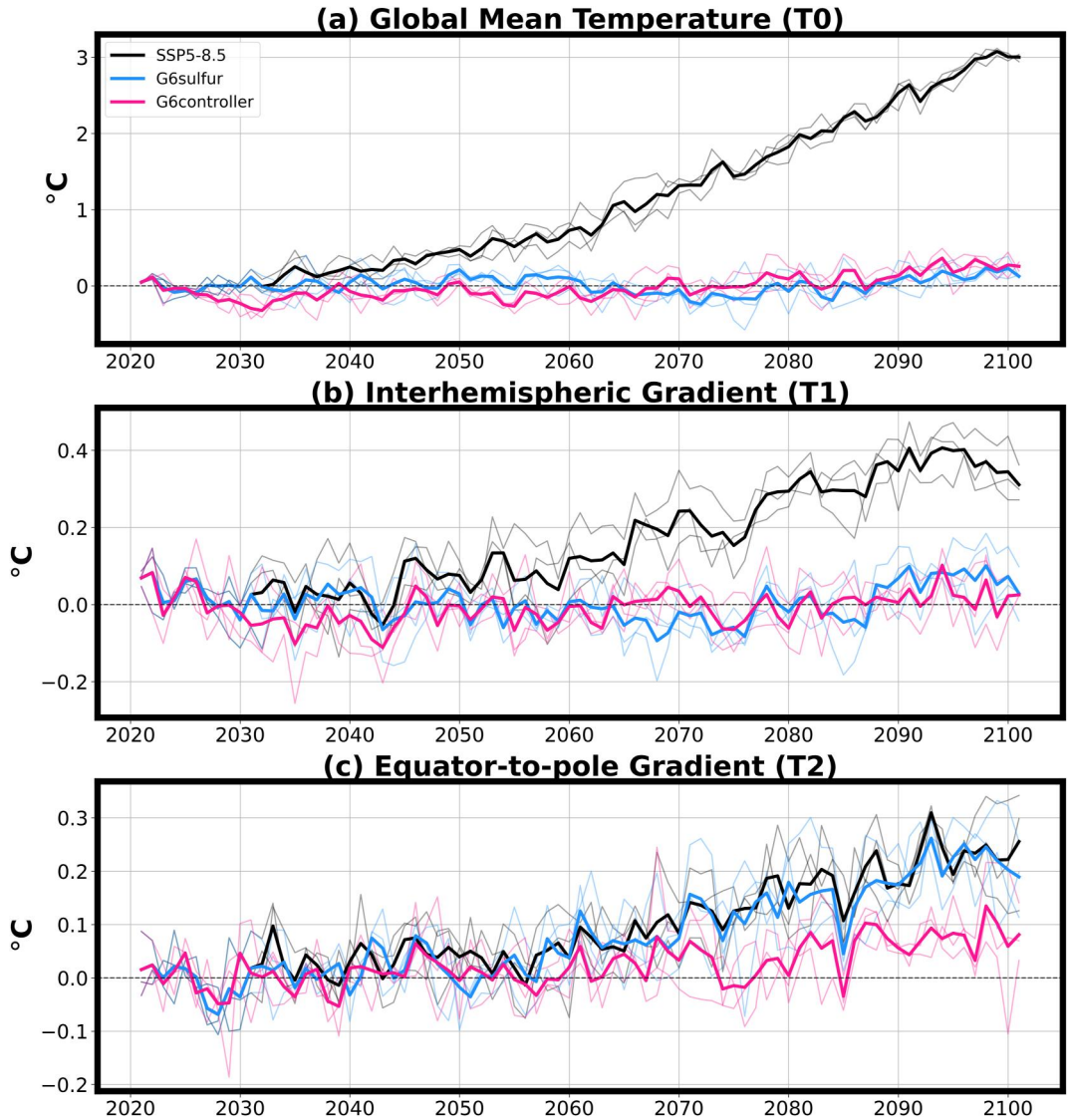

Figure 2. Changes in annual mean (a) global mean temperature, T0 (b) interhemispheric gradient, T1 (c) equator-to-pole gradient, T2 for SSP5-8.5 (black), G6sulfur (blue), G6controller (pink) compared to those in the SSP2-4.5 scenario. The thick lines represent the ensemble mean, whereas thin lines show each ensemble member.

equator-to-pole gradient (T_2). These targets correspond to the values simulated in the SSP2-4.5 warming scenario, as per the G6 scenario design. As seen in Figure 2a, both simulations reduce the global mean surface air temperature by 3°C by the end of the century. G6controller is also designed to meet T_1 and T_2. Whilst the G6sulfur strategy was not designed to meet the T_1 temperature target, both injection strategies in fact meet this target relatively well. This was also true in CESM1 (Kravitz et al., 2019) however, similar simulations in CESM2 do not meet the T_1 target (Zhang et al., 2024), suggesting that this result is model dependent.

Regarding T_2, SSP5-8.5 shows a substantial weakening in the magnitude of the (negative) equator-to-pole gradient over the twenty-first century, which is caused by the strong arctic amplification commonly found in UKESM1 under increasing GHG emissions (e.g., Henry et al., 2023; Swaminathan et al., 2022). G6controller meets the T_2 target relatively well during the first 60 years of the simulation, although a small bias emerges over the final 20 years. G6sulfur, however, does not meet the T_2 target (it was not designed to). The driving factor in the weakening of the equator-to-pole temperature gradient in G6sulfur compared to G6controller is the difference in the distribution of stratospheric aerosol. Figure 3a shows the end of the century zonal stratospheric aerosol optical depth (sAOD) in both G6sulfur and G6controller. The sAOD in G6sulfur is mainly confined to the tropical region

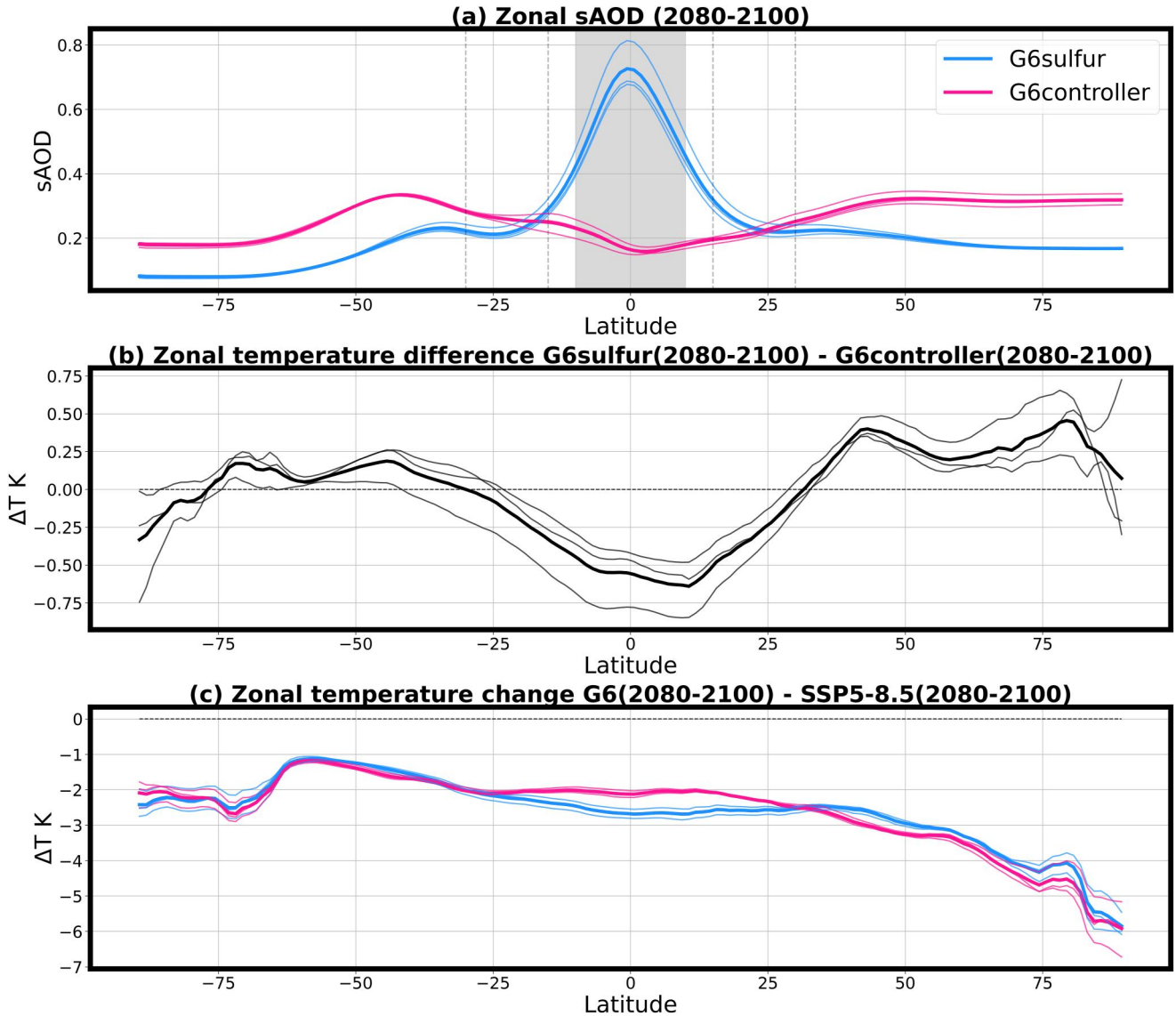

Figure 3. (a) Zonal mean stratospheric aerosol optical depth in G6sulfur (blue) and G6controller (pink). The shaded region between 10°N and 10°S represents the injection location for G6sulfur and the vertical dashed lines at 30°S, 15°S, 15°N, and 30°N show the injection locations for G6controller. (b) Zonal mean temperature difference between G6sulfur and G6controller. (c) Zonal mean temperature changes in G6sulfur (blue) and G6controller (pink) relative to the SSP5-8.5 scenario. The thick lines represent the ensemble mean, whereas thin lines show each ensemble member.

with limited dispersion toward the poles as aerosols are confined inside the tropical pipe. As such, the peak sAOD values (0.45) simulated in the narrow band around the equator are over double those seen at high latitudes. In contrast, stratospheric aerosols are much more dispersed under G6controller, with substantially higher sAOD values over the midlatitudes and the poles.

Model intercomparisons have previously highlighted a stronger confinement of aerosols in the tropical stratosphere in UKESM1 compared to other models (Bednarz et al., 2023c; Visioni et al., 2021, 2023a). This implies stronger vertical advection within the tropical pipe and strengthened transport barriers, potentially influencing both transport dynamics and aerosol microphysics. Between 10°N and 10°S the sAOD in G6sulfur is over four times greater than G6controller whilst at most other latitudes the sAOD in G6sulfur is only around half of that in G6controller (Figure 3a). This is reflected in the latitudinal pattern of zonal temperature difference between G6sulfur and G6controller (Figure 3b). The overall latitudinal pattern of cooling relative to SSP5-8.5 is similar in the two injection strategies (Figure 3c), with the greatest cooling simulated in the Arctic, however, there are

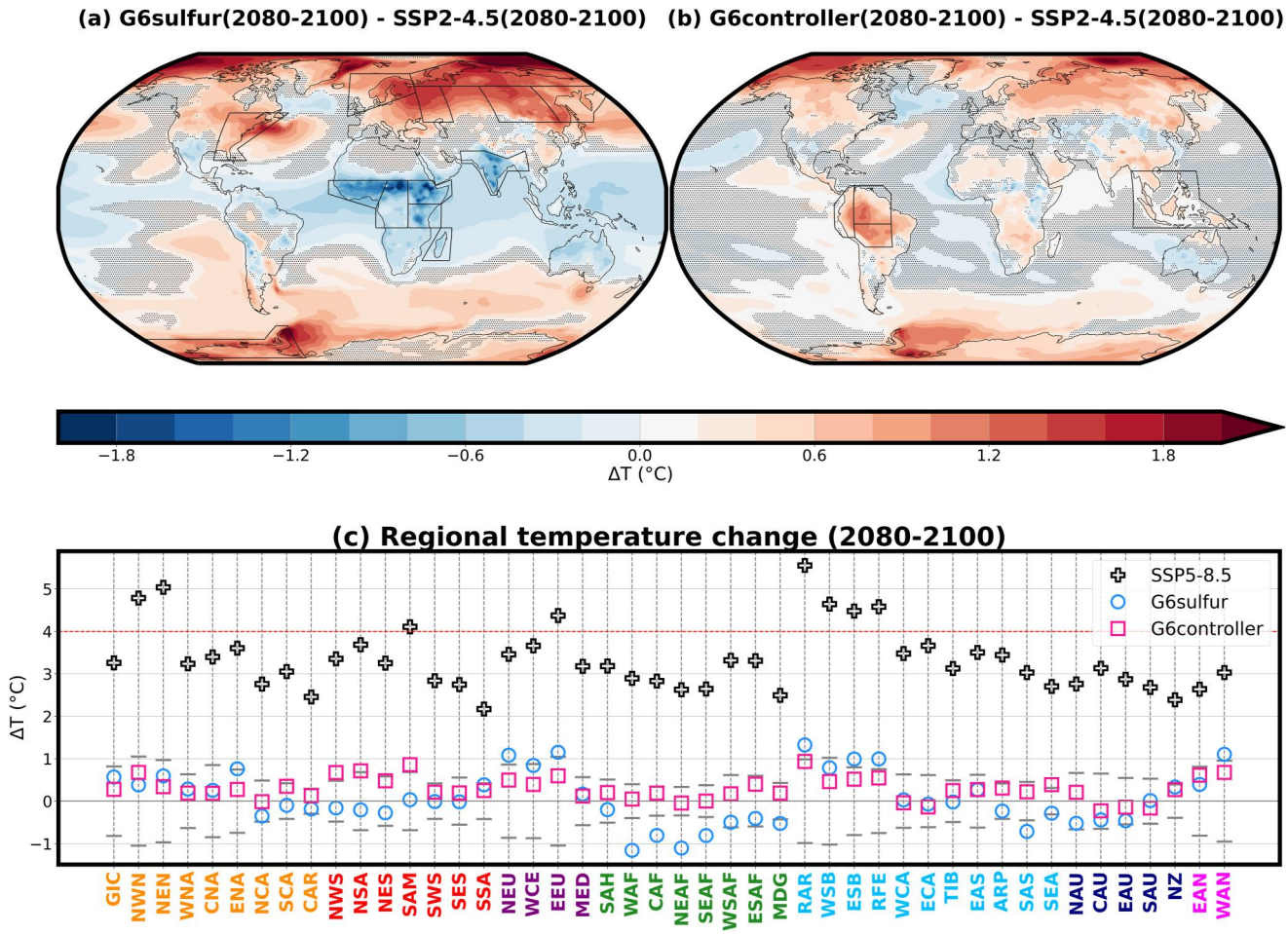

Figure 4. (a, b) Annual surface air temperature change in the ensemble-mean averaged over 2080–2100 for (a) G6sulfur and (b) G6controller relative to the SSP2-4.5 ensemble mean in the same time period. Regions outlined in black represent the AR6 land-only regions where the regional mean surface air temperature change was greater than one standard deviation of the SSP2-4.5 regional mean. Shaded areas indicate where the difference is not statistically significant, as evaluated using a double-sided *t*-test with $p < 0.05$ considering all ensemble members and 20 years as independent samples. (c) Regional temperature change relative to SSP2-4.5 (gray markers represent ±1 std derived from SSP2-4.5, red dashed line 4°C).

significant differences between injection strategies in surface temperature relative to the target, SSP2-4.5, scenario (Figure 3b). This supports results from Henry et al. (2023) indicating that the latitudinal pattern of the SAI-induced surface cooling relative to the baseline scenario in UKESM is not dominated by the latitudinal pattern of the direct radiative forcing from stratospheric aerosol but rather this model's internal climate feedbacks.

4. Surface Air Temperature Changes

Even though both injection strategies meet the same global mean near-surface air temperature target, large differences in the regional temperature response between the SSP2-4.5 and SAI scenarios are simulated, in agreement with the previous CESM SAI studies (e.g., Kravitz et al., 2019; Zhang et al., 2024). This is illustrated in Figure 4 with significant differences between the end of the century (2081–2100) G6 and SSP2-4.5 temperatures across the two injection strategies. Under G6sulfur, the large stratospheric aerosol burden across the equatorial region results in a tropical cooling relative to SSP2-4.5 exceeding 1.5°C in places. There is also a residual warming in the polar regions, in some places exceeding 1.5°C, with greater warming seen in the Arctic than the Antarctic. As aforementioned, this regional disparity drives the weakening of the equator-to-pole gradient (i.e., an increase in T_2 in Figure 2c) under an equatorial injection.

Under the multi-latitude injection strategy, G6controller, the sAOD is more evenly distributed across both hemispheres (Figure 3a) and results in a more homogeneous temperature response. There are fewer AR6 regions (12% of regions in G6controller vs. 25% in G6sulfur) which experience a significant cooling relative to SSP2-4.5 (Figure 4c). Nonetheless, a similar pattern of residual warming is found across the poles, especially in the Arctic, although reduced in magnitude. Additionally, G6controller is unable to cool the Amazon (NSA, NES, SAM) to within the range of variability (±1 std) of the target, whereas G6sulfur does. This is in part due to a greater warming in this region under SSP5-8.5 that cannot be fully mitigated under this SAI strategy (Figure 4c, Figure S2 in Supporting Information S1), and the comparatively lower sAOD in G6controller over this region compared to G6sulfur (Figure S3 in Supporting Information S1).

Figure 4c highlights the regions where the surface air temperature over land is outside of the range of variability (±1 std) of the SSP2-4.5 warming scenario (as illustrated by gray markers). In both strategies the AR6 regions across northern Eurasia (EEU, RAR, WSB, ESB, RFE for G6sulfur; RAR, ESB, RFE for G6controller) exceed this threshold, owing to the high arctic amplification in UKESM1 under the SSP5-8.5 GHG scenario that cannot be fully mitigated with these SAI strategies (see also Pan et al., 2023; Swaminathan et al., 2022).

In addition, in G6controller half of the AR6 regions experiencing statistically significant temperature changes also experience a particularly strong regional warming under SSP5-8.5 (e.g., North America [NWN], central South America [SAM], and northern Russia [RAR, ESB, RFE]; Figure 4c) that is not fully offset under SAI in this strategy. For G6sulfur, on the other hand, these regions are more widespread and largely located in the tropics as a result of the "overcooling" from the high stratospheric aerosol burden. Henry et al. (2023) found a similar temperature response to those seen in G6controller, noting that the Arctic warming occurs mostly in winter (December, January, February [DJF]) (Henry et al., 2023; Figure S3 in Supporting Information S1).

It is clear from Figure 4 that a multi-latitude injection strategy such as G6controller is better able to balance the "overcooling" that has been previously observed from the early equatorial SAI strategies (e.g., Kravitz et al., 2019; Laakso et al., 2017) and is able to reduce residual warming of the poles. Unlike the previous studies, however, we have also shown that this strategy leads to the undercooling of the Amazon and, to a lesser extent, the undercooling of land regions of the maritime continent in UKESM1.

5. Changes in Precipitation and Its Drivers

5.1. Precipitation Response

While the global mean temperatures in G6sulfur and G6controller are, by design, maintained at SSP2-4.5 levels, global mean precipitation is reduced compared to SSP2-4.5. Previous studies have shown that SRM exhibits a different hydrological sensitivity to GHG forcings (e.g., Bala et al., 2008; Kleidon et al., 2015; Niemeier et al., 2013) and that changes in both large scale and regional tropospheric circulation (e.g., Cheng et al., 2022; Simpson et al., 2019) and the combined effects of these on the hydrological cycle and regional precipitation are uncertain (Ricke et al., 2023; Tilmes et al., 2013). Our results show that global mean precipitation under both G6 strategies increases at a similar rate to SSP2-4.5 for the first 20 years of the simulations but subsequently diverge. The global mean precipitation under G6sulfur decreases slightly post 2050 and then stabilizes for the final 30 years, whilst under G6controller it continues to increase throughout the twenty-first century albeit at a slower rate than in SSP2-4.5. Averaged over the last two decades (2080–2100) this corresponds to the global mean decrease of 0.14 mm day^{-1} (−4%) for G6sulfur and 0.09 mm day^{-1} (−2.7%) for G6controller relative to SSP2-4.5 in the same period (Figure 5a).

Similarly to the surface air temperature response, the regional pattern of precipitation change is heterogeneous. Figures 5b–5d show the end of the century (2080–2100) mean precipitation relative to SSP2-4.5 for SSP5-8.5, G6sulfur and G6controller. In the high emissions scenario, SSP5-8.5, whilst global mean precipitation increases, there is a significant decrease in precipitation over the Amazon region and over southern Europe. Regions which experience the largest mean increase in precipitation relative to SSP2-4.5 include East Africa, the Tibetan Plateau and Indonesia. As in Figure 4, land regions outside of the range of variability (±1 std) of SSP2-4.5 have been highlighted.

As expected from the global mean, G6sulfur shows large areas of decreased precipitation, mainly throughout the tropical region but also across large areas of Eurasia and North America. The reduction of precipitation around the equator in G6sulfur, accompanied by the increase in precipitation in the subtropics, reflects a weakening of the

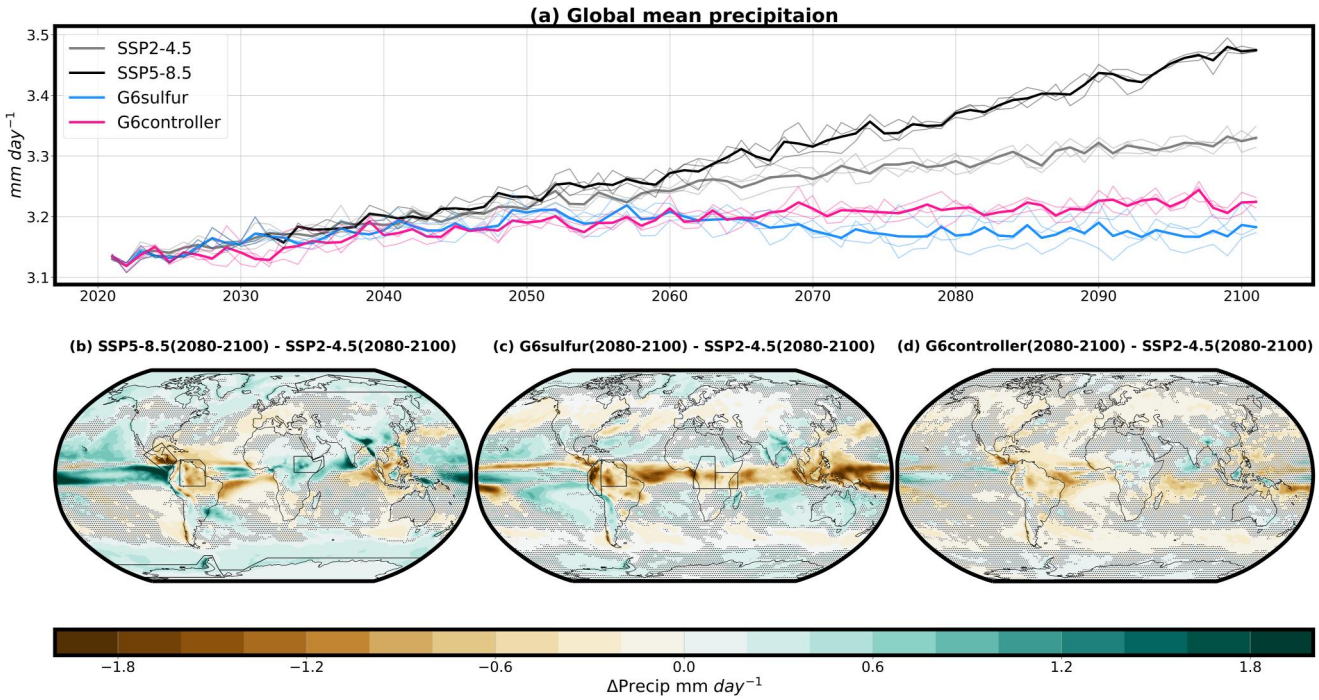

Figure 5. (a) Global mean precipitation for SSP2-4.5 (gray), SSP5-8.5 (black), G6sulfur (blue) and G6controller (pink). The thick lines represent the ensemble mean, whereas thin lines show each ensemble member. (b–d) Annual precipitation change in the ensemble-mean averaged over 2080–2100 for (b) SSP5-8.5, (c) G6sulfur and (d) G6controller relative to the SSP2-4.5 ensemble mean in the same time period. Regions outlined in black represent the AR6 land-only regions where the change in the regional mean precipitation was greater than one standard deviation of the SSP2-4.5 regional mean. Shaded areas indicate where the difference is not statistically significant, as evaluated using a double-sided *t*-test with $p < 0.05$ considering all ensemble members and 20 years as independent samples.

intensity of Hadley Circulation (Section 5.2). This weakening is one of the key drivers in the greater reduction of precipitation over the Amazon in G6sulfur compared to that under SSP5-8.5 and G6controller. The distribution of sAOD in G6sulfur (Figure S1 in Supporting Information S1), compared to G6controller, results in a strong reduction in surface solar radiation across the tropics. This reduces the surface sensible and latent heat fluxes, increasing the stability of the atmosphere and inhibiting convection, contributing to the weakening of the Hadley Circulation and therefore a reduction in tropical precipitation (Schneider et al., 2010).

Changes in precipitation under G6controller are found to be smaller compared to G6sulfur, with less statistical significance over both land and ocean regions and with fewer AR6 regions outside the range of variability in SSP2-4.5 (black boxes in Figures 5b–5d). While the G6controller strategy does show some statistically significant increases in precipitation over Bangladesh, the increase is much reduced compared to that found in either SSP5-8.5 or G6sulfur. The spatial pattern of precipitation change over land in G6controller is mostly similar to that of G6sulfur but is of a smaller magnitude. An exception to this are the precipitation changes over the Maritime Continent, whereby precipitation decreases over land in this region in G6sulfur by 0.58 mm day^{-1} but increases in G6controller by 0.17 mm day^{-1}.

G6controller was designed to minimize changes in the interhemispheric temperature difference (T_1) to minimize large scale shifts in the ITCZ (e.g., Haywood et al., 2013) that are controlled by the strength of the cross-equatorial flows of energy and moisture (e.g., Frierson et al., 2013). G6sulfur also meets this target despite no explicit design choice (Figure 2b), however there are greater differences in the precipitation response under G6sulfur, especially in the tropical region. This can be examined further by looking at the seasonal precipitation cycle and changes to large-scale tropospheric circulations.

For many regions, especially in the tropics, the seasonal precipitation change is more relevant than the annual mean owing to the influence of the seasonal monsoons. From June until September the summer monsoon rains occur over South Asian countries, whereas from December until February the monsoon rains shift south of the equator toward Australia and the Maritime Continent. Changes in monsoon patterns have huge implications on

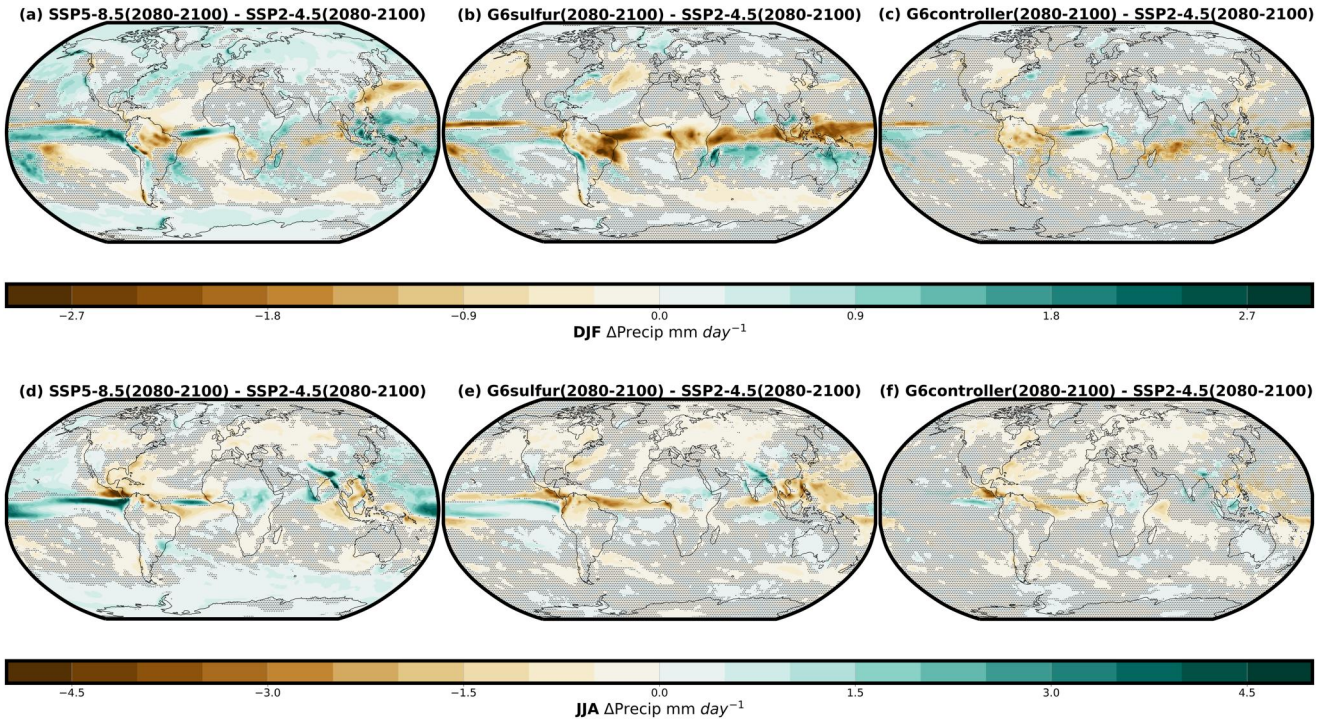

Figure 6. Seasonal precipitation change in the ensemble-mean averaged over December, January, February (DJF) and June, July, August (JJA) 2080–2100 for (a, d) SSP5-8.5, (b, e) G6sulfur and (c, f) G6controller relative to the SSP2-4.5 ensemble mean in the same time period. Regions outlined in black represent the AR6 land-only regions where the change in the regional mean precipitation was greater than one standard deviation of the SSP2-4.5 regional mean. Shaded areas indicate where the difference is not statistically significant, as evaluated using a double-sided *t*-test with $p < 0.05$ considering all ensemble members and 20 years as independent samples.

agriculture, economy and health. Figure 6 shows the end of century (2080–2100) seasonal (December, January, February [DJF]; June, July, August [JJA]) precipitation change relative to SSP2-4.5 for SSP5-8.5, G6sulfur and G6controller. An increase in monsoon precipitation over the Maritime Continent in DJF and over the Tibetan Plateau in JJA dominates the signal in SSP5-8.5. The decrease in precipitation over the Amazon mostly occurs during DJF, the southern hemisphere summer. This feature is also seen in both G6 strategies, however in G6sulfur the decrease (1.05 mm day^{-1}) is double that of both SSP5-8.5 (0.50 mm day^{-1}) and G6controller (0.58 mm day^{-1}). In G6sulfur the reduction in tropical precipitation is greater in DJF than JJA and reflects changes to the Hadley circulation (Section 5.2). Similarly to the annual mean, changes to seasonal precipitation in G6controller are much smaller and less significant.

5.2. Large-Scale Tropospheric Circulation Changes

The Hadley circulation is a large-scale tropical atmospheric circulation with rising air at the equator diverging poleward in the upper troposphere and descending in the subtropics. The structure and behavior of the Hadley circulation can greatly influence global climate, playing an important role in forming tropical and subtropical climatic zones. The warm and humid converging air in the ascending branches of the Hadley circulation forms the ITCZ, with its associated heavy precipitation, whilst the sinking branches consist of mainly dry air and, thus, are associated with little rainfall, resulting in large arid regions within the subtropics. Some studies have reported a weakening in the Hadley circulation intensity with increased GHGs (e.g., Lu et al., 2007; Ma et al., 2012) although Vallis et al. (2015) found some disagreement within CMIP5 models in the southern hemisphere Hadley circulation during JJA and observations show a poleward expansion of the circulation (Staten et al., 2018; Waugh et al., 2018). Since changes to precipitation patterns in the tropics could have large impacts on food and water security for many people (Wheeler & Von Braun, 2013), it is important to assess how SAI could impact these circulation changes.

To assess changes in the Hadley circulation intensity under the GHG induced warming and the SAI scenarios we calculate the meridional mass stream function following the formula in Haigh et al. (2005). SSP2-4.5 shows the

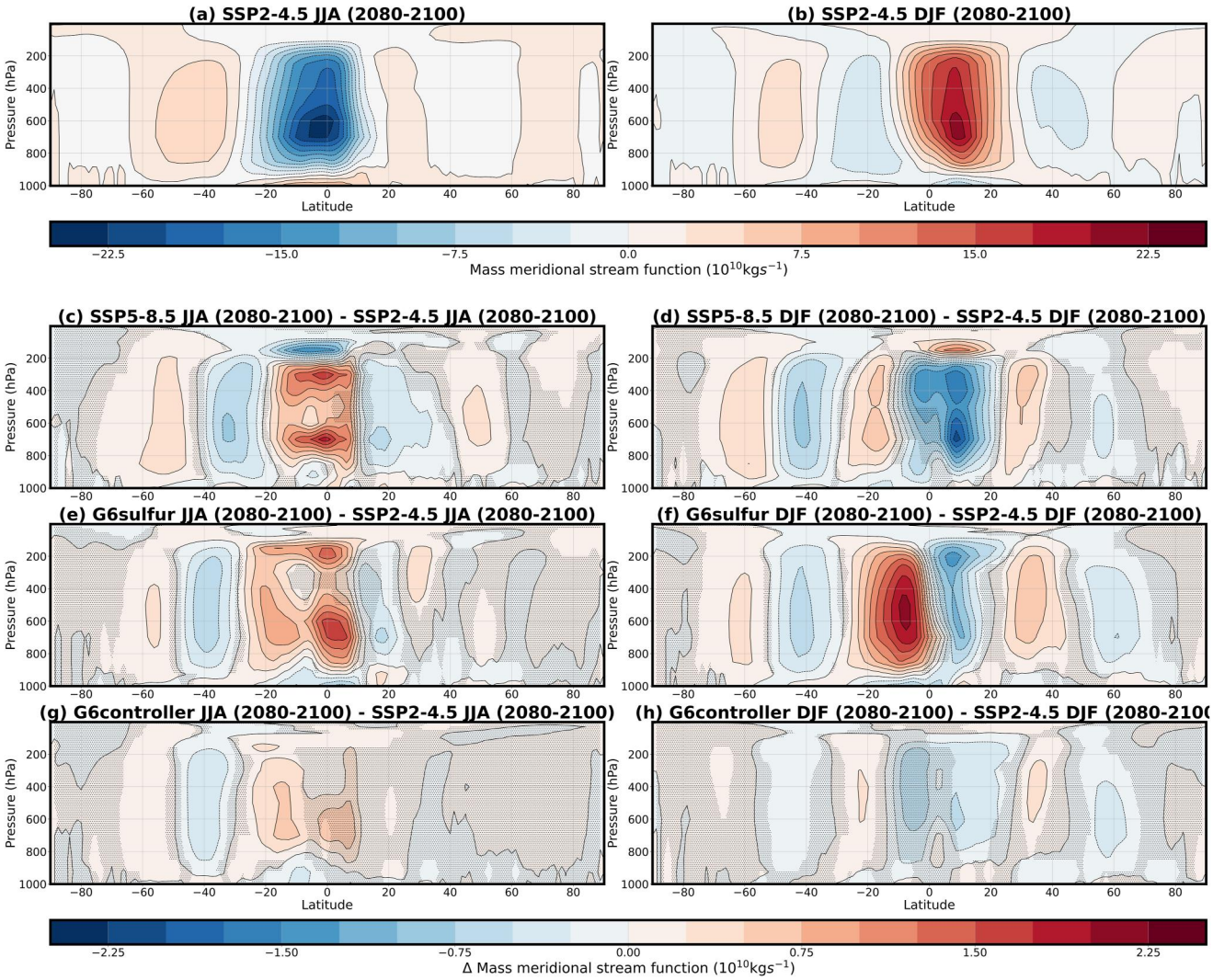

Figure 7. Zonal and ensemble mean meridional mass stream function (10^{10} kg s^{-1}) in June, July, August (JJA) (a, c, e, g) and December, January, February (DJF) (b, d, f, h) averaged over the years 2080–2100 for SSP2-4.5 (a, b) and the difference in meridional mass stream function for (c, d) SSP5-8.5, (e, f) G6sulfur and (g, h) G6controller relative to the SSP2-4.5 scenario. Red indicates a clockwise rotation and blue indicates an anticlockwise rotation. Shaded areas indicate where the difference is not statistically significant, as evaluated using a double-sided *t*-test with $p < 0.05$ considering all ensemble members and 20 years as independent samples.

typical anticlockwise rotation in the southern hemisphere cell and a clockwise rotation in the northern hemisphere cell, with both the position and intensity of the two cells varying between winter and summer (Figures 7a and 7b).

Figures 7c–7h shows the difference in the DJF and JJA meridional mass stream function relative to SSP2-4.5 for SSP5-8.5, G6sulfur and G6controller. SSP5-8.5 shows a significantly weaker Hadley circulation in both hemispheres compared to SSP2-4.5, which is consistent with the literature (e.g., Vallis et al., 2015). In DJF, G6sulfur shows a significant change to the northern Hadley circulation cell compared to SSP2-4.5, with the amplitude of the stream function maximum at 500 hPa decreasing by 5%. This is associated with a significant reduction (~20%) of the vertical velocity at the equator, contributing to the reduction of precipitation in the tropical region (Figure 6b), and a significant increase in vertical velocity (~9%) around the downward branch (not shown). We also note that the descending branch of the northern Hadley circulation shifts poleward, therefore widening the Hadley circulation and shifting the subtropical dry zone polewards, contributing to the significant decrease in precipitation around continental Asia (Figure 6b). In contrast, while some weakening of the northern Hadley circulation occurs in DJF under G6controller, the response is much weaker and not significant.

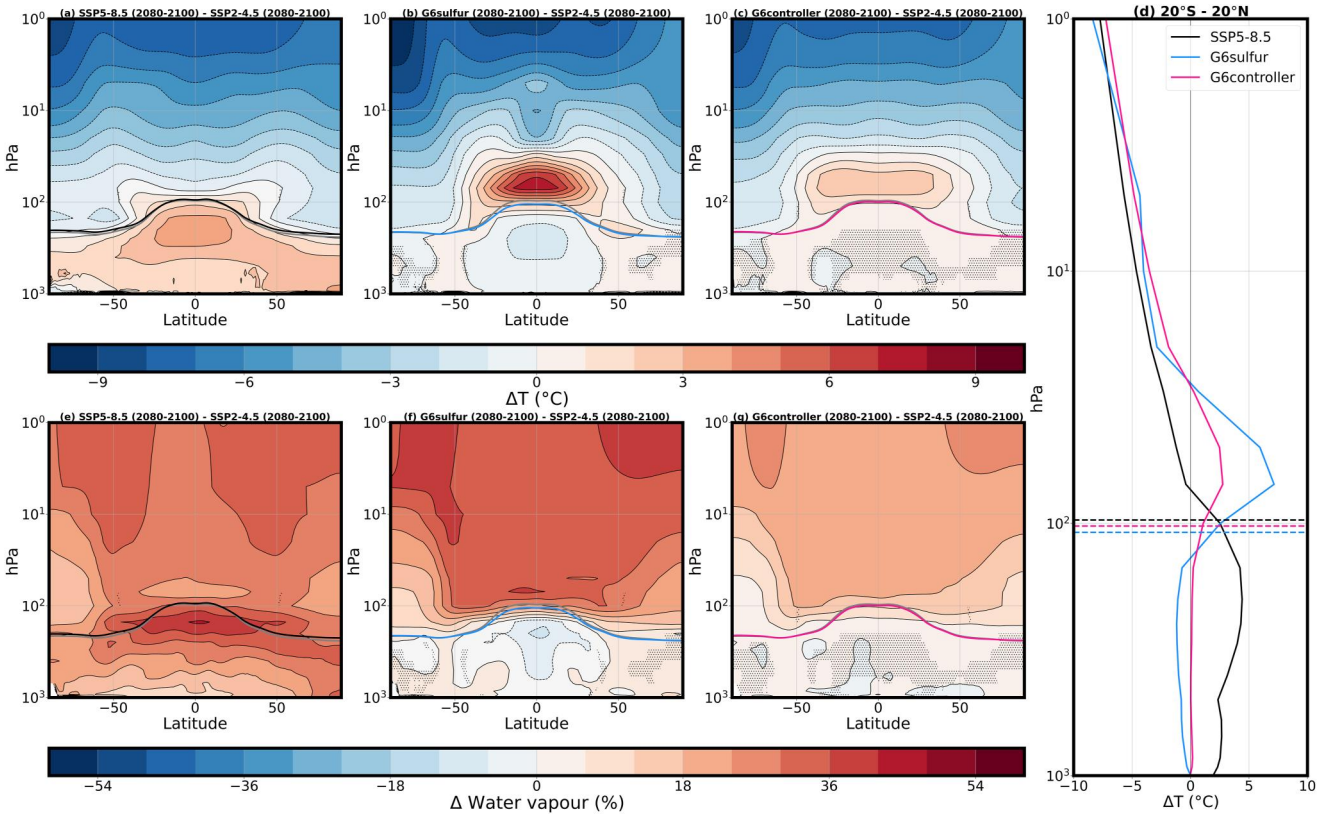

Figure 8. (a)–(c) Zonal mean temperature change in the ensemble-mean averaged over 2080–2100 for (a) SSP5-8.5, (b) G6sulfur and (c) G6controller relative to the SSP2-4.5 ensemble mean in the same period. (d) Zonal and ensemble mean temperature averaged over 20°S–20°N and 2080–2100 for SSP5-8.5 (black), G6sulfur (blue) and G6controller (pink) relative to the SSP2-4.5 scenario. (e)–(f) Zonal mean percentage change of water vapor in the ensemble-mean averaged over 2080–2100 for (e) SSP5-8.5, (f) G6sulfur and (g) G6controller relative to the SSP2-4.5 ensemble mean in the same period. The solid lines on (a, b, c, e, f, g) and dashed lines on (d) indicate the tropopause height for SSP2-4.5 (gray), SSP5-8.5 (black), G6sulfur (blue) and G6controller (pink). Shaded areas indicate where the difference is not statistically significant, as evaluated using a double-sided *t*-test with $p < 0.05$ considering all ensemble members and 20 years as independent samples.

In JJA the response under G6controller is similar to the DJF response, that is, a slight decrease of Hadley circulation intensity with little statistical significance in the upward branch. Under G6sulfur we see a similar response to that of SSP5-8.5 with a decrease in Hadley circulation intensity, although unlike the DJF response there is little change in the width of the Hadley circulation.

Changes in the Hadley circulation intensity are often explained in terms of the associated changes in meridional temperature gradients, troposphere static stability and tropopause height (e.g., Held, 2000; Seo et al., 2014). As we discussed in Section 3, the meridional temperature gradient in G6controller is relatively well maintained throughout the simulations compared to the equatorial injection strategy G6sulfur which was not designed to meet this target and thus results in the anomalous weakening of the gradient of around 0.2°C relative to the target by the end of the century. In addition, the magnitude of the deceleration in upwelling in the tropical troposphere is smaller in G6controller than in G6sulfur. This deceleration is caused by an increase in static stability associated with lower stratospheric heating and tropospheric cooling which occurs in the tropics under G6sulfur but less so in G6controller (Figures 8b and 8c). Finally, changes in the tropical tropospheric and lower stratospheric temperatures in G6sulfur lead to the lowering of the tropopause height compared to the SSP2-4.5 target, the magnitude of which becomes much smaller in G6controller (Figure 8d), we see a 10% decrease in the altitude of the tropopause height between G6sulfur and G6controller, with only a very small decrease (3.5%) between G6controller and the target, SSP2-4.5.

These results agree with other studies assessing changes to the Hadley circulation under different injection strategies (Bednarz et al., 2023a; Cheng et al., 2022). Cheng et al. (2022) compared Hadley circulation intensity in the CESM1 simulations in the GLENS and the equivalent equatorial injection strategy defined in Bednarz

et al. (2023a) and Kravitz et al. (2019) compared an equatorial injection with multiple symmetric off-equatorial strategies in CESM2, with both studies reporting a similar result.

We note that SAI-induced changes in surface energy fluxes are only one of the possible drivers of the simulated large-scale circulation and precipitation changes, and their dependence on the SAI strategy. Simpson et al. (2019) examined the precipitation response to stratospheric heating in the CESM1 model and found some significant changes, particularly in tropical precipitation with wet regions getting drier and dry regions getting wetter, suggesting that the top-down influence of the SAI-induced lower stratospheric heating on tropospheric circulation and precipitation could also play a role here. Note that Simpson et al. (2019) apply a tropical stratospheric heating that is approximately twice as strong as that modeled here in the G6sulfur simulations (Section 6.1), and that they acknowledge that the specific feedback mechanisms linking stratospheric heating to precipitation changes are not well understood.

6. Stratospheric Response

6.1. Stratospheric Temperatures

One of the important impacts of SAI to consider is the stratospheric heating induced by the introduction of sulfate aerosols. Since sulfate is not purely scattering at wavelengths longer than approximately 1.4 μm (e.g., Dykema et al., 2016; Haywood et al., 2022), the partial absorption of solar and terrestrial radiation by aerosols results in stratospheric heating. Previous studies have investigated the role of stratospheric heating in contributing to climate impacts from SAI, including changes in stratospheric and tropospheric circulation and the resulting modulation of global and regional precipitation patterns (Cheng et al., 2022; Simpson et al., 2019; Visioni et al., 2020).

Figures 8a–8c shows the difference in zonal mean temperature (2080–2100) relative to SSP2-4.5 for SSP5-8.5, G6sulfur and G6controller. In agreement with previous studies (e.g., Cheng et al., 2022; Kravitz et al., 2019), tropospheric temperatures increase under the high GHG scenario (SSP5-8.5), with a maximum in the tropical upper troposphere and a small warming extending up to the tropical lower stratosphere. Both G6 SAI strategies show temperature increases in the extra-polar lower stratosphere, with G6sulfur warming the tropical stratosphere (20°S–20°N) by 66% more than G6controller (Figure 8d). The larger amplitude of the tropical lower stratospheric heating in G6sulfur compared to G6controller results from the combination of much higher sulfate concentrations simulated within the tropics (Figure S4 in Supporting Information S1; Figure 3a; see also Bednarz et al., 2023a; Kravitz et al., 2019) as well as the lower altitude of SO_2 injection (see also Lee et al., 2023).

Warming in the tropical lower stratosphere in both G6 strategies is associated with warming and lowering of the tropical tropopause. This allows for an increase in stratospheric water vapor (Figures 8e–8g), which acts to offset the direct aerosol-induced surface cooling (Bednarz et al., 2023a; Haywood et al., 2022; Lee et al., 2023) as well as modulating stratospheric temperatures and ozone concentrations (Maycock et al., 2013; Tilmes et al., 2021).

In comparison, the magnitude of the lower stratospheric warming and the resulting increase in stratospheric water vapor in G6controller is much reduced compared to G6sulfur. The latter is also partially related to the lower altitude of the SO_2 injection in G6sulfur (18–20 km) compared to G6controller (21.5 km), thereby resulting in larger impacts on tropopause temperatures, in agreement with the results of Lee et al. (2023).

6.2. Stratospheric Ozone

Changes to stratospheric temperatures as a result of SAI can drive changes in stratospheric ozone, due to changes in both stratospheric dynamics and chemistry. Studies have shown that enhancements of the stratospheric sulfate aerosol layer from SAI would increase the aerosol surface area density, influencing halogen activation in the lower stratosphere and the removal of active nitrogen species in the middle stratosphere, thereby modulating chemical ozone loss (Bednarz et al., 2023a, 2023b; Haywood et al., 2022; Tilmes et al., 2018a, 2022). In addition, the SAI-induced lower stratospheric heating will also influence ozone via changes in the large scale transport as well as through increased stratospheric water vapor levels and thus chemical ozone loss.

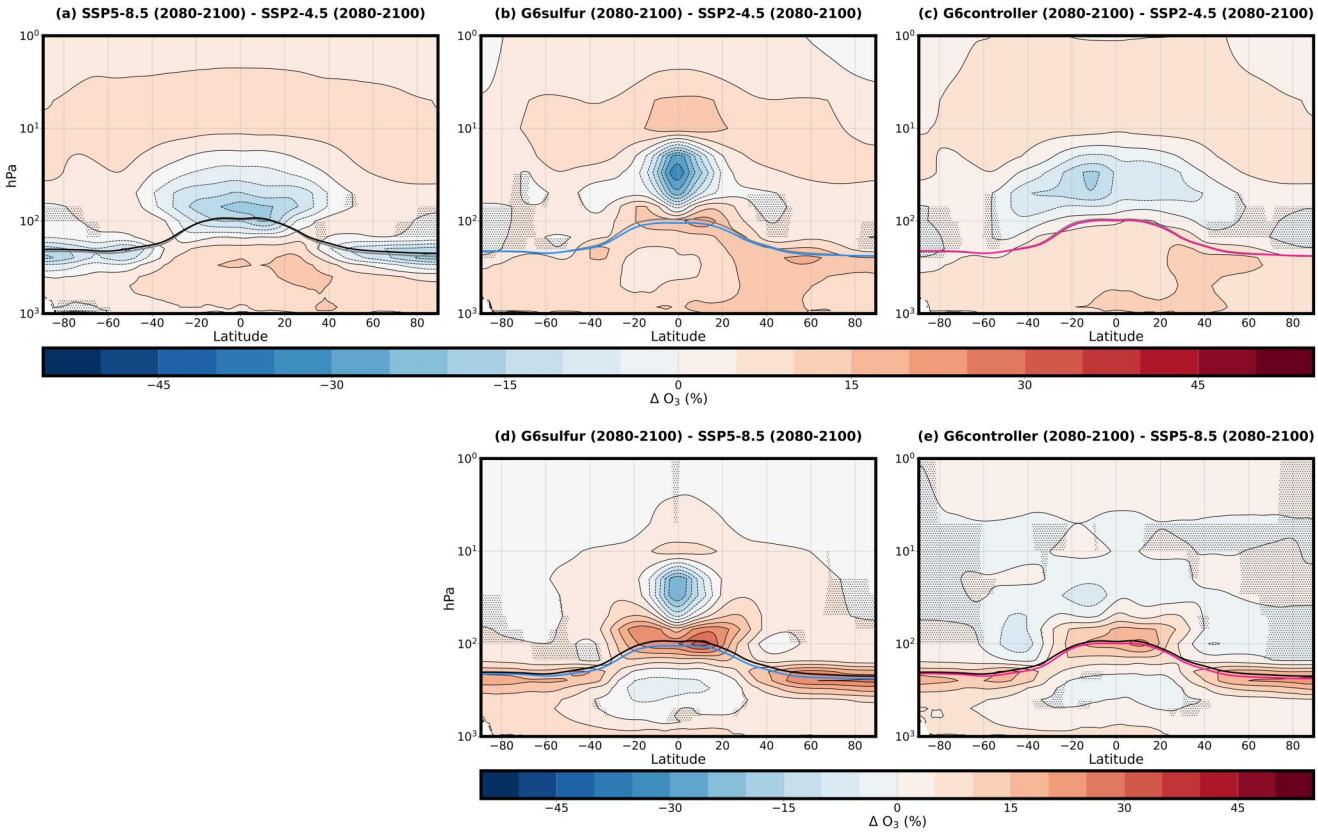

Figure 9. Zonal mean percentage difference of ozone in the ensemble-mean averaged over 2080–2100 for (a) SSP5-8.5, (b) G6sulfur and (c) G6controller relative to SSP2-4.5 in the same period and (d) G6sulfur and (e) G6controller relative to SSP5-8.5 in the same period. The solid lines indicate the tropopause height for SSP2-4.5 (gray), SSP5-8.5 (black), G6sulfur (blue) and G6controller (pink). Shaded areas indicate where the difference is not statistically significant, as evaluated using a double-sided *t*-test with $p < 0.05$ considering all ensemble members and 20 years as independent samples.

Figures 9a–9c shows the percentage change of ozone relative to SSP2-4.5 for SSP5-8.5, G6sulfur and G6controller. We see a general decrease of ozone under SSP5-8.5 around the tropopause at most latitudes as the result of the GHG-induced increase in tropopause height relative to SSP2-4.5. Ozone also decreases in SSP5-8.5 in the tropical lower stratosphere, likely as the result of the GHG-induced strengthening of the Brewer-Dobson Circulation (BDC), and the resulting dynamically-induced ozone reduction as more ozone-poor air is transported from the troposphere. In addition, higher stratospheric H_2O (Figure 8e) owing to higher methane emissions in SSP5-8.5 acts to enhance the HOx-mediated chemical ozone loss throughout the stratosphere, and this effect can thus contribute to the ozone decrease simulated in the tropical lower stratosphere. In the upper stratosphere, where chemical timescales are much faster than dynamical timescales, SSP5-8.5 shows increased ozone throughout the globe compared to the SSP2-4.5. The response results from the GHG-induced stratospheric cooling and the resulting declaration of the catalytic chemical ozone loss in that region.

In order to isolate the purely SAI-induced response from those arising from the GHG-induced changes in stratospheric temperatures, chemistry and transport (which was also evident in the SSP5-8.5 response in Figures 9a), Figures 9d–9e compares the percentage change of ozone in both G6 strategies relative to SSP5-8.5. Both G6 strategies show significant ozone increases around the tropopause throughout the globe as the result of the SAI-induced lowering of the tropopause height (Section 6.1).

In G6sulfur, there are also further ozone increases in the subtropical lower stratosphere and an ozone decrease in the equatorial stratosphere above it. The response likely results from the SAI-induced changes in circulation, with the deceleration of the shallow branch of the BDC and upwelling in the tropical upper troposphere and lower stratosphere (reducing the transport of ozone-poor air into the lower stratosphere) and acceleration of the deep BDC branch (enhancing the transport of ozone-poor tropical lower stratospheric air into the middle stratosphere above the aerosol layer), in a manner similar to that in previous CESM studies (Bednarz et al., 2023a; Tilmes

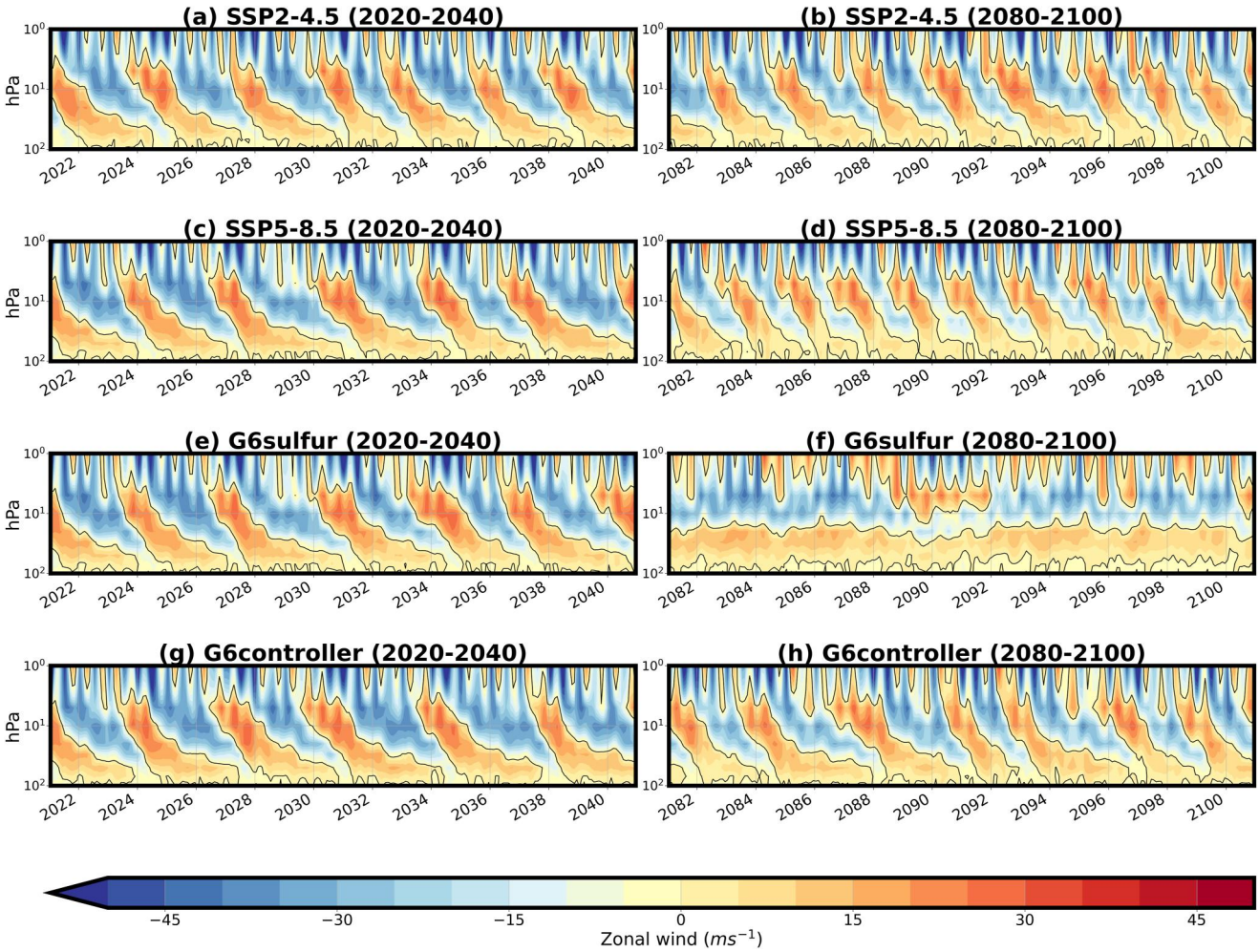

Figure 10. Zonal mean winds of one ensemble member averaged over 5°S–5°N as a function of time (months) over 2020–2040 (a, c, e, g) and 2080–2100 (b, d, f, h) for (a, b) SSP2-4.5, (c, d) SSP5-8.5, (e, f) G6sulfur and (g, h) G6controller.

et al., 2018b). In contrast, these ozone changes are much reduced in G6controller, likely as the result of the much reduced stratospheric heating (Figure 8c) and, thus, changes in stratospheric circulation and transport. As discussed in Haywood et al. (2022), the spatial distribution of sulfate aerosol strongly influences changes in transport which is the largest difference between G6sulfur and G6controller in this case.

6.3. Quasi-Biennial Oscillation

The Quasi-Biennial Oscillation (QBO) is an easterly and westerly oscillation of the equatorial zonal winds in the tropical stratosphere. Aquila et al. (2014) first reported changes to the period and amplitude of the QBO under equatorial injections of sulfur into the stratosphere. They found that for large increases in stratospheric aerosol burden (5Tg SO_2) the QBO would be locked into a permanent westerly phase. This occurs as the increased stratospheric warming disturbs the thermal wind balance and increases the residual vertical velocity (Niemeier et al., 2011) resulting in an additional westerly component of the zonal wind above the heated aerosol layer, and thus delayed descent of the westerly QBO phase (Figure S5 in Supporting Information S1) (Aquila et al., 2014; Niemeier & Schmidt, 2017). In addition, in the westerly phase of the QBO there is equatorward motion which results in stronger aerosol confinement in the tropical pipe where mixing is strongly constrained (Niemeier & Schmidt, 2017; Punge et al., 2009; Visioni et al., 2018).

Figure 10 shows the first and last 20 years of the QBO for one ensemble member of the SSP2-4.5, SSP5-8.5, G6sulfur and G6controller simulations. Under global warming we see some changes to the period and amplitude

of oscillation, in particular the shortening of its period, more pronounced under the high emissions scenario SSP5-8.5. Similarly to previous studies (Aquila et al., 2014; Bednarz et al., 2023a; Kravitz et al., 2019) the strong tropical lower stratospheric warming under G6sulfur leads to locking of the QBO into a permanent westerly phase by the end of the century (G6sulfur, Figure 10f, Figure S5 in Supporting Information S1). Despite some noticeable changes to the oscillation relative to SSP2-4.5, including weakening of its amplitude and elongation of its period, the QBO is not entirely disrupted under G6controller when the aerosol is injected away from the equator, supporting results from similar comparative studies with the CESM model (e.g., Bednarz et al., 2023c; Kravitz et al., 2019).

7. Conclusions

In this study we have compared the climate impacts of two SAI strategies using the UKESM1 earth system model under the GeoMIP G6 scenario, both reducing global mean near-surface air temperatures from the SSP5-8.5 levels to those of SSP2-4.5, that is, by 3°C by the end of the century. G6sulfur, a quasi- equatorial injection at 18–20 km between 10°N and 10°S, with the injection amount manually adjusted every decade, and G6controller, a feedback-controlled multi-latitude injection strategy (30°S, 15°S, 15°N and 30°N) at 21.5 km with the global mean surface air temperature and the interhemispheric and equator-to-pole gradients as its targets. Similar comparisons had previously only been performed in two versions of the same model (CESM1; Kravitz et al., 2019; CESM2; Zhang et al., 2024). Our study therefore provides insight into how the climate responds in UKESM1 under these two different injection strategies, allowing us to begin to understand which climate responses are consistent under SAI and which are more strategy and/or model dependent.

G6sulfur exhibits the robust tropospheric temperature response consisting of "overcooling" of the tropics and "undercooling" of the poles typical to previous equatorial SAI strategies (e.g., Kravitz et al., 2019). This is a result of the latitudinal distribution of stratospheric aerosols which are mostly confined inside the tropical pipe with little dispersion toward the mid-latitudes. Similar tropical overcooling is not observed under G6controller which has a more homogenous surface air temperature response relative to the SSP2-4.5 target. In the high latitudes, however, the latitudinal pattern of surface cooling relative to the baseline scenario SSP5-8.5 is similar in both injection strategies, with the greatest cooling occurring in the northern high latitudes. Henry et al. (2023) found similar results under the ARISE-SAI-1.5 simulations in UKESM1 and suggested that this surface cooling is more dependent on the model's climate feedbacks rather than latitudinal distribution of the direct radiative forcing, a result that is consistent across injection strategies in this model.

There is a widely acknowledged disagreement among climate models regarding regional precipitation changes in a warming climate (Masson-Delmotte et al., 2021). This disparity significantly contributes to the range of projections concerning both large-scale and regional changes in the water cycle. Therefore, the impact of SAI on regional and extreme precipitation is still very uncertain (Ricke et al., 2023), however our results are consistent with previous studies which suggest that global-mean precipitation is suppressed under SAI compared to that in the target period. Furthermore, there is a greater reduction in the global and tropical precipitation under G6sulfur than under G6controller, potentially impacting the water and food security of many people living in these regions (Wheeler & Von Braun, 2013). There are several contributing factors to the decrease in tropical precipitation, some of which are still poorly understood. Our analysis suggests that under G6sulfur the larger decrease in downward shortwave radiation in the tropics compared to G6controller could certainly contribute to the weakening of the Hadley Circulation and thus suppress precipitation in for example, the Amazon or central African region through changes in the surface energy budget, although dynamically induced changes in tropospheric circulation could also play a role (e.g., Simpson et al., 2019). However, it is important to note that significant differences in the sign of tropical precipitation change between CESM2 and UKESM1 have been observed, specifically over India and the Tibetan Plateau (see Figures 6 and 8; Henry et al., 2023) which highlights the need for more model intercomparisons and more in depth mechanistic understanding of the key processes involved to determine what would be a robust hydrological response to SAI. Whilst efforts were made to further investigate the role of stratospheric heating on precipitation in the G6 scenarios using idealized simulations, this is an area outside of the scope of this study and will be pursued in future work.

The role of stratospheric heating in the climate response to SAI is complex and needs to be better understood to reduce uncertainty in the model's response. This study showed that the choice to move the injection location away from equator can decrease tropical stratospheric heating by 66% and therefore reduce the impact on the large scale

atmospheric dynamics, including the Hadley Circulation (Cheng et al., 2022) and the QBO (Kravitz et al., 2019). Our results showed a significant change to the northern and southern hemisphere Hadley circulation in G6sulfur with poleward shifts of the northern downward branch and a significant weakening of intensity in both hemispheres. Results from G6controller revealed that the weakening of the Hadley cells under SSP5-8.5 could be reduced under this injection strategy. We also showed that the increased stratospheric heating in G6sulfur compared to G6controller contributed to the locking of the westerly phase of the QBO, similar to previous studies (e.g., Aquila et al., 2014; Kravitz et al., 2019).

The results of this study highlight the effectiveness of the 4-latitude injection strategy, G6controller, in reducing global mean temperatures by 3°C, whilst mitigating the negative consequences associated with equatorial injection strategies, such as G6sulfur. Although the targets T_0, T_1, and T_2 of the G6controller are temperature-based, the benefits of the control algorithm extend beyond temperatures due to associated dynamical feedbacks. Specifically, (a) tropical precipitation is less impacted, due to more limited effects on the Hadley circulation, (b) the tropical stratosphere warms less, leading to less impact on tropical stratospheric ozone concentrations, and (c) the reduction in tropical stratospheric heating under G6controller minimizes impacts on the QBO.

While similar comparisons have been made in other climate models, a comprehensive analysis of an off-equatorial injection strategy across multiple modeling centers is essential to identify commonalities and uncertainties. It's worth noting that the latitudinal injection strategy determined by the controller differs significantly from that of Henry et al. (2023), where the T_0, T_1, and T_2 targets were fixed at +1.5°C above model pre-industrial conditions, without temporal target evolution. Furthermore, even with the same scenario and climate targets, injection strategies needed to achieve those targets vary significantly across different climate models, as highlighted by Henry et al. (2023). A new GeoMIP experiment proposed by Visioni et al. (2023c) injecting at 30°N and 30°S to meet 1.5°C above pre-industrial under SSP2-4.5 will allow for further exploration of the impacts of an off-equatorial SAI strategy across more modeling centers. Determining which strategy best represents the real world remains an open question, emphasizing the need for further research in SAI to unravel the complexities and interplay between SAI emissions, forcing patterns, and climate responses. Future work will delve into the differences in extreme events between the two G6 strategies and explore the role of stratospheric heating in G6sulfur.

Data Availability Statement

The processed model output used throughout this work are available on Zenodo (Wells, Jones, & Dalvi, 2023; https://doi.org/10.5281/zenodo.10302574) and code for reproducibility is available on GitHub (Wells, Henry, & Bednarz, 2023; https://doi.org/10.5281/zenodo.10302916).

Acknowledgments
Alice Florence Wells, James Matthew Haywood, Matthew Henry, Andy Jones, and Mohit Dalvi were supported by SilverLining through its Safe Climate Research Initiative. James Matthew Haywood, Andy Jones, and Mohit Dalvi were also supported by the Met Office Hadley Centre Climate Programme funded by DESNZ. James Matthew Haywood and Matthew Henry were further supported by the NERC EXTEND project (NE/W003880/1). Alice Florence Wells was further supported by a UKRI Centre for Doctoral Training in Environmental Intelligence PhD studentship hosted by the University of Exeter (NE/T006897/1). Support for Ewa M. Bednarz has been provided by the National Oceanic and Atmospheric Administration (NOAA) cooperative agreement NA22OAR4320151, and the Earth Radiative Budget initiative. Support for Douglas G. MacMartin has been provided by the Atkinson Center for Sustainability at Cornell University and the National Science Foundation through agreement CBET-2038246.

References

Aquila, V., Garfinkel, C., Newman, P., Oman, L., & Waugh, D. (2014). Modifications of the quasi-biennial oscillation by a geoengineering perturbation of the stratospheric aerosol layer. *Geophysical Research Letters*, *41*(5), 1738–1744. https://doi.org/10.1002/2013GL058818

Archibald, A. T., O'Connor, F. M., Abraham, N. L., Archer-Nicholls, S., Chipperfield, M. P., Dalvi, M., et al. (2020). Description and evaluation of the UKCA stratosphere–troposphere chemistry scheme (StratTrop vn 1.0) implemented in UKESM1. *Geoscientific Model Development*, *13*(3), 1223–1266. https://doi.org/10.5194/gmd-13-1223-2020

Bala, G., Duffy, P., & Taylor, K. (2008). Impact of geoengineering schemes on the global hydrological cycle. *Proceedings of the National Academy of Sciences*, *105*(22), 7664–7669. https://doi.org/10.1073/pnas.0711648105

Bednarz, E. M., Butler, A. H., Visioni, D., Zhang, Y., Kravitz, B., & MacMartin, D. G. (2023a). Injection strategy–a driver of atmospheric circulation and ozone response to stratospheric aerosol geoengineering. *Atmospheric Chemistry and Physics*, *23*(21), 13665–13684. https://doi.org/10.5194/acp-23-13665-2023

Bednarz, E. M., Visioni, D., Butler, A. H., Kravitz, B., MacMartin, D. G., & Tilmes, S. (2023b). Potential non-linearities in the high latitude circulation and ozone response to stratospheric aerosol injection. *Geophysical Research Letters*, *50*(22), e2023GL104726. https://doi.org/10.5194/acp-23-687-2023

Bednarz, E. M., Visioni, D., Kravitz, B., Jones, A., Haywood, J. M., Richter, J., et al. (2023c). Climate response to off-equatorial stratospheric sulfur injections in three Earth System Models–Part 2: Stratospheric and free-tropospheric response. *Atmospheric Chemistry and Physics*, *23*(1), 687–709. https://doi.org/10.1029/2023GL104726

Best, M. J., Pryor, M., Clark, D., Rooney, G. G., Essery, R., Ménard, C., et al. (2011). The joint UK land environment simulator (JULES), model description–Part 1: Energy and water fluxes. *Geoscientific Model Development*, *4*(3), 677–699. https://doi.org/10.5194/gmd-4-677-2011

Brody, E., Visioni, D., Bednarz, E. M., Kravitz, B., MacMartin, D. G., Richter, J. H., & Tye, M. R. (2024). Kicking the can down the road: Understanding the effects of delaying the deployment of stratospheric aerosol injection (Version 1). *arXiv*. https://doi.org/10.48550/ARXIV.2402.11992

Budyko, M. I. (1977). On present-day climatic changes. *Tellus*, *29*(3), 193–204. https://doi.org/10.1111/j.2153-3490.1977.tb00725.x

Cheng, W., MacMartin, D. G., Kravitz, B., Visioni, D., Bednarz, E. M., Xu, Y., et al. (2022). Changes in Hadley circulation and intertropical convergence zone under strategic stratospheric aerosol geoengineering. *npj Climate and Atmospheric Science*, *5*(1), 32. https://doi.org/10.1038/s41612-022-00254-6

Crutzen, P. J. (2006). Albedo enhancement by stratospheric sulfur injections: A contribution to resolve a policy dilemma? *Climatic Change*, *77*(3–4), 211. https://doi.org/10.1007/s10584-006-9101-y

Dhomse, S. S., Mann, G. W., Antuña Marrero, J. C., Shallcross, S. E., Chipperfield, M. P., Carslaw, K. S., et al. (2020). Evaluating the simulated radiative forcings, aerosol properties, and stratospheric warmings from the 1963 Mt Agung, 1982 El Chichón, and 1991 Mt Pinatubo volcanic aerosol clouds. *Atmospheric Chemistry and Physics*, *20*(21), 13627–13654. https://doi.org/10.5194/acp-20-13627-2020

Dykema, J. A., Keith, D. W., & Keutsch, F. N. (2016). Improved aerosol radiative properties as a foundation for solar geoengineering risk assessment. *Geophysical Research Letters*, *43*(14), 7758–7766. https://doi.org/10.1002/2016GL069258

Fasullo, J. T., & Richter, J. H. (2023). Dependence of strategic solar climate intervention on background scenario and model physics. *Atmospheric Chemistry and Physics*, *23*(1), 163–182. https://doi.org/10.5194/acp-23-163-2023

Franke, H., Niemeier, U., & Visioni, D. (2021). Differences in the quasi-biennial oscillation response to stratospheric aerosol modification depending on injection strategy and species. *Atmospheric Chemistry and Physics*, *21*(11), 8615–8635. https://doi.org/10.5194/acp-21-8615-2021

Frierson, D. M., Hwang, Y.-T., Fučkar, N. S., Seager, R., Kang, S. M., Donohoe, A., et al. (2013). Contribution of ocean overturning circulation to tropical rainfall peak in the northern hemisphere. *Nature Geoscience*, *6*(11), 940–944. https://doi.org/10.1038/ngeo1987

Haigh, J. D., Blackburn, M., & Day, R. (2005). The response of tropospheric circulation to perturbations in lower-stratospheric temperature. *Journal of Climate*, *18*(17), 3672–3685. https://doi.org/10.1175/JCLI3472.1

Haywood, J. M., Jones, A., Bellouin, N., & Stephenson, D. (2013). Asymmetric forcing from stratospheric aerosols impacts Sahelian rainfall. *Nature Climate Change*, *3*(7), 660–665. https://doi.org/10.1038/nclimate1857

Haywood, J. M., Jones, A., Johnson, B. T., & McFarlane Smith, W. (2022). Assessing the consequences of including aerosol absorption in potential stratospheric aerosol injection climate intervention strategies. *Atmospheric Chemistry and Physics*, *22*(9), 6135–6150. https://doi.org/10.5194/acp-22-6135-2022

Haywood, J. M., Jones, A., Jones, A. C., Halloran, P., & Rasch, P. J. (2023). Climate intervention using marine cloud brightening (MCB) compared with stratospheric aerosol injection (SAI) in the UKESM1 climate model. *Atmospheric Chemistry and Physics*, *23*(24), 15305–-15324. https://doi.org/10.5194/acp-23-15305-2023

Haywood, J. M., Tilmes, S., Jones, A., Keutsch, F., Laakso, A., Niemeier, U., et al. (2022). Stratospheric aerosol injection and its potential effect on the stratospheric ozone layer. In *Scientific assessment of ozone depletion: 2022* (pp. 325–383). World Meteorological Organization.

Heckendorn, P., Weisenstein, D., Fueglistaler, S., Luo, B. P., Rozanov, E., Schraner, M., et al. (2009). The impact of geoengineering aerosols on stratospheric temperature and ozone. *Environmental Research Letters*, *4*(4), 045108. https://doi.org/10.1088/1748-9326/4/4/045108

Held, I. M. (2000). The general circulation of the atmosphere. [Conference Paper].

Henry, M., Haywood, J., Jones, A., Dalvi, M., Wells, A., Visioni, D., et al. (2023). Comparison of UKESM1 and CESM2 simulations using the same multi-target stratospheric aerosol injection strategy. *Atmospheric Chemistry and Physics*, *23*(20), 13369–13385. https://doi.org/10.5194/acp-23-13369-2023

Hueholt, D. M., Barnes, E. A., Hurrell, J. W., Richter, J. H., & Sun, L. (2023). Assessing outcomes in stratospheric aerosol injection scenarios shortly after deployment. *Earth's Future*, *11*(5), e2023EF003488. https://doi.org/10.1029/2023EF003488

Iturbide, M., Gutiérrez, J. M., Alves, L. M., Bedia, J., Cimadevilla, E., Cofiño, A. S., et al. (2020). An update of IPCC climate reference regions for subcontinental analysis of climate model data: Definition and aggregated datasets. *Earth System Science Data Discussions*, *2020*(4), 1–16. https://doi.org/10.5194/essd-12-2959-2020

Jones, A., Haywood, J., Boucher, O., Kravitz, B., & Robock, A. (2010). Geoengineering by stratospheric SO_2 injection: Results from the Met Office HadGEM2 climate model and comparison with the Goddard Institute for Space Studies ModelE. *Atmospheric Chemistry and Physics*, *10*(13), 5999–6006. https://doi.org/10.5194/acp-10-5999-2010

Jones, A., Haywood, J. M., Jones, A. C., Tilmes, S., Kravitz, B., & Robock, A. (2020). North Atlantic Oscillation response in GeoMIP experiments G6solar and G6sulfur: Why detailed modelling is needed for understanding regional implications of solar radiation management. https://doi.org/10.5194/acp-21-1287-2021

Jones, A. C., Haywood, J. M., Dunstone, N., Emanuel, K., Hawcroft, M. K., Hodges, K. I., & Jones, A. (2017). Impacts of hemispheric solar geoengineering on tropical cyclone frequency. *Nature Communications*, *8*(1), 1382. https://doi.org/10.1038/s41467-017-01606-0

Jones, A. C., Haywood, J. M., Jones, A., & Aquila, V. (2016). Sensitivity of volcanic aerosol dispersion to meteorological conditions: A Pinatubo case study. *Journal of Geophysical Research: Atmospheres*, *121*(12), 6892–6908. https://doi.org/10.1002/2016JD025001

Kleidon, A., Kravitz, B., & Renner, M. (2015). The hydrological sensitivity to global warming and solar geoengineering derived from thermodynamic constraints. *Geophysical Research Letters*, *42*(1), 138–144. https://doi.org/10.1002/2014GL062589

Kravitz, B., Caldeira, K., Boucher, O., Robock, A., Rasch, P. J., Alterskjaer, K., et al. (2013). Climate model response from the geoengineering model intercomparison project (GeoMIP). *Journal of Geophysical Research: Atmospheres*, *118*(15), 8320–8332. https://doi.org/10.1002/jgrd.50646

Kravitz, B., MacMartin, D. G., Mills, M. J., Richter, J. H., Tilmes, S., Lamarque, J.-F., et al. (2017). First simulations of designing stratospheric sulfate aerosol geoengineering to meet multiple simultaneous climate objectives. *Journal of Geophysical Research: Atmospheres*, *122*(23), 12–616. https://doi.org/10.1002/2017JD026874

Kravitz, B., MacMartin, D. G., Tilmes, S., Richter, J. H., Mills, M. J., Cheng, W., et al. (2019). Comparing surface and stratospheric impacts of geoengineering with different SO_2 injection strategies. *Journal of Geophysical Research: Atmospheres*, *124*(14), 7900–7918. https://doi.org/10.1029/2019JD030329

Kravitz, B., MacMartin, D. G., Wang, H., & Rasch, P. J. (2016). Geoengineering as a design problem. *Earth System Dynamics*, *7*(2), 469–497. https://doi.org/10.5194/esd-7-469-2016

Kravitz, B., Robock, A., Tilmes, S., Boucher, O., English, J. M., Irvine, P. J., et al. (2015). The geoengineering model intercomparison project phase 6 (GeoMIP6): Simulation design and preliminary results. *Geoscientific Model Development*, *8*(10), 3379–3392. https://doi.org/10.5194/gmd-8-3379-2015

Laakso, A., Korhonen, H., Romakkaniemi, S., & Kokkola, H. (2017). Radiative and climate effects of stratospheric sulfur geoengineering using seasonally varying injection areas. *Atmospheric Chemistry and Physics*, *17*(11), 6957–6974. https://doi.org/10.5194/acp-17-6957-2017

Lee, W. R., Visioni, D., Bednarz, E. M., MacMartin, D. G., Kravitz, B., & Tilmes, S. (2023). Quantifying the efficiency of stratospheric aerosol geoengineering at different altitudes. *Geophysical Research Letters*, *50*(14), e2023GL104417. https://doi.org/10.1029/2023GL104417

Lu, J., Vecchi, G. A., & Reichler, T. (2007). Expansion of the Hadley cell under global warming. *Geophysical Research Letters*, *34*, L06805. https://doi.org/10.1029/2006gl028443

Ma, J., Xie, S.-P., & Kosaka, Y. (2012). Mechanisms for tropical tropospheric circulation change in response to global warming. *Journal of Climate*, *25*(8), 2979–2994. https://doi.org/10.1175/JCLI-D-11-00048.1

MacMartin, D. G., & Kravitz, B. (2019). The engineering of climate engineering. *Annual Review of Control, Robotics, and Autonomous Systems*, *2*(1), 445–467. https://doi.org/10.1146/annurev-control-053018-023725

MacMartin, D. G., Kravitz, B., Long, J. C., & Rasch, P. J. (2016). Geoengineering with stratospheric aerosols: What do we not know after a decade of research? *Earth's Future*, *4*(11), 543–548. https://doi.org/10.1002/2016EF000418

MacMartin, D. G., Kravitz, B., Tilmes, S., Richter, J. H., Mills, M. J., Lamarque, J.-F., et al. (2017). The climate response to stratospheric aerosol geoengineering can be tailored using multiple injection locations. *Journal of Geophysical Research: Atmospheres*, *122*(23), 12–574. https://doi.org/10.1002/2017JD026868

MacMartin, D. G., Ricke, K. L., & Keith, D. W. (2018). Solar geoengineering as part of an overall strategy for meeting the 1.5 C Paris target. *Philosophical Transactions of the Royal Society A: Mathematical, Physical and Engineering Sciences*, *376*(2119), 20160454. https://doi.org/10.1098/rsta.2016.0454

MacMartin, D. G., Visioni, D., Kravitz, B., Richter, J., Felgenhauer, T., Lee, W., et al. (2022). Scenarios for modeling solar radiation modification. *Proceedings of the National Academy of Sciences*, *119*(33), e2202230119. https://doi.org/10.1073/pnas.2202230119

Mann, G., Carslaw, K., Ridley, D., Spracklen, D., Pringle, K., Merikanto, J., et al. (2012). Intercomparison of modal and sectional aerosol microphysics representations within the same 3-D global chemical transport model. *Atmospheric Chemistry and Physics*, *12*(10), 4449–4476. https://doi.org/10.5194/acp-12-4449-2012

Mann, G., Carslaw, K., Spracklen, D., Ridley, D., Manktelow, P., Chipperfield, M., et al. (2010). Description and evaluation of GLOMAP-mode: A modal global aerosol microphysics model for the UKCA composition-climate model. *Geoscientific Model Development*, *3*(2), 519–551. https://doi.org/10.5194/gmd-3-519-2010

Masson-Delmotte, V., Zhai, P., Pirani, A., Connors, S. L., Péan, C., Berger, S., et al. (2021). IPCC, 2021: Summary for policymakers climate change 2021: The physical science basis. Contribution of Working Group I to the sixth assessment report of the Intergovernmental Panel on Climate Change.

Maycock, A. C., Joshi, M. M., Shine, K. P., & Scaife, A. A. (2013). The circulation response to idealized changes in stratospheric water vapor. *Journal of Climate*, *26*(2), 545–561. https://doi.org/10.1175/JCLI-D-12-00155.1

NASEM, National Academies of Sciences, Engineering and Medicine. (2021). *Reflecting sunlight: Recommendations for solar geoengineering research and research governance*. National Academies Press. https://doi.org/10.17226/25762

Niemeier, U., & Schmidt, H. (2017). Changing transport processes in the stratosphere by radiative heating of sulfate aerosols. *Atmospheric Chemistry and Physics*, *17*(24), 14871–14886. https://doi.org/10.5194/acp-17-14871-2017

Niemeier, U., Schmidt, H., Alterskjær, K., & Kristjánsson, J. (2013). Solar irradiance reduction via climate engineering: Impact of different techniques on the energy balance and the hydrological cycle. *Journal of Geophysical Research: Atmospheres*, *118*(21), 11–905. https://doi.org/10.1002/2013JD020445

Niemeier, U., Schmidt, H., & Timmreck, C. (2011). The dependency of geoengineered sulfate aerosol on the emission strategy. *Atmospheric Science Letters*, *12*(2), 189–194. https://doi.org/10.1002/asl.304

Niemeier, U., & Timmreck, C. (2015). What is the limit of climate engineering by stratospheric injection of SO_2? *Atmospheric Chemistry and Physics*, *15*(16), 9129–9141. https://doi.org/10.5194/acp-15-9129-2015

O'Neill, B. C., Tebaldi, C., Van Vuuren, D. P., Eyring, V., Friedlingstein, P., Hurtt, G., et al. (2016). The scenario model intercomparison project (ScenarioMIP) for CMIP6. *Geoscientific Model Development*, *9*(9), 3461–3482. https://doi.org/10.5194/gmd-9-3461-2016

Pan, R., Shu, Q., Wang, Q., Wang, S., Song, Z., He, Y., & Qiao, F. (2023). Future Arctic climate change in CMIP6 strikingly intensified by nemo-family climate models. *Geophysical Research Letters*, *50*(4), e2022GL102077. https://doi.org/10.1029/2022GL102077

Punge, H., Konopka, P., Giorgetta, M., & Müller, R. (2009). Effects of the quasi-biennial oscillation on low-latitude transport in the stratosphere derived from trajectory calculations. *Journal of Geophysical Research*, *114*(D3), D03102. https://doi.org/10.1029/2008JD010518

Rasch, P. J., Tilmes, S., Turco, R. P., Robock, A., Oman, L., Chen, C.-C., et al. (2008). An overview of geoengineering of climate using stratospheric sulphate aerosols. *Philosophical Transactions of the Royal Society A: Mathematical, Physical and Engineering Sciences*, *366*(1882), 4007–4037. https://doi.org/10.1098/rsta.2008.0131

Richter, J. H., Visioni, D., MacMartin, D. G., Bailey, D. A., Rosenbloom, N., Dobbins, B., et al. (2022). Assessing responses and impacts of solar climate intervention on the earth system with stratospheric aerosol injection (ARISE-SAI): Protocol and initial results from the first simulations. *Geoscientific Model Development*, *15*(22), 8221–8243. https://doi.org/10.5194/gmd-15-8221-2022

Ricke, K., Wan, J. S., Saenger, M., & Lutsko, N. J. (2023). Hydrological consequences of solar geoengineering. *Annual Review of Earth and Planetary Sciences*, *51*(1), 447–470. https://doi.org/10.1146/annurev-earth-031920-083456

Ridley, J. K., Blockley, E. W., Keen, A. B., Rae, J. G., West, A. E., & Schroeder, D. (2018). The sea ice model component of HadGEM3-GC3. 1. *Geoscientific Model Development*, *11*(2), 713–723. https://doi.org/10.5194/gmd-11-713-2018

Robock, A., MacMartin, D. G., Duren, R., & Christensen, M. W. (2013). Studying geoengineering with natural and anthropogenic analogs. *Climatic Change*, *121*(3), 445–458. https://doi.org/10.1007/s10584-013-0777-5

Schneider, T., O'Gorman, P. A., & Levine, X. J. (2010). Water vapor and the dynamics of climate changes. *Reviews of Geophysics*, *48*(3), RG3001. https://doi.org/10.1029/2009RG000302

Sellar, A. A., Jones, C. G., Mulcahy, J. P., Tang, Y., Yool, A., Wiltshire, A., et al. (2019). UKESM1: Description and evaluation of the UK earth system model. *Journal of Advances in Modeling Earth Systems*, *11*(12), 4513–4558. https://doi.org/10.1029/2019MS001739

Seneviratne, S. I., Zhang, X., Adnan, M., Badi, W., Dereczynski, C., Di Luca, A., et al. (2021). Weather and climate extreme events in a changing climate. (Chapter 11). https://doi.org/10.1017/9781009157896.013

Seo, K.-H., Frierson, D. M., & Son, J.-H. (2014). A mechanism for future changes in Hadley circulation strength in CMIP5 climate change simulations. *Geophysical Research Letters*, *41*(14), 5251–5258. https://doi.org/10.1002/2014GL060868

Simpson, I., Tilmes, S., Richter, J., Kravitz, B., MacMartin, D., Mills, M. J., et al. (2019). The regional hydroclimate response to stratospheric sulfate geoengineering and the role of stratospheric heating. *Journal of Geophysical Research: Atmospheres*, *124*(23), 12587–12616. https://doi.org/10.1029/2019JD031093

Staten, P. W., Lu, J., Grise, K. M., Davis, S. M., & Birner, T. (2018). Re-examining tropical expansion. *Nature Climate Change*, *8*(9), 768–775. https://doi.org/10.1038/s41558-018-0246-2

Storkey, D., Blaker, A. T., Mathiot, P., Megann, A., Aksenov, Y., Blockley, E. W., et al. (2018). UK global ocean GO6 and GO7: A traceable hierarchy of model resolutions. *Geoscientific Model Development*, *11*(8), 3187–3213. https://doi.org/10.5194/gmd-11-3187-2018

Swaminathan, R., Parker, R. J., Jones, C. G., Allan, R. P., Quaife, T., Kelley, D. I., et al. (2022). The physical climate at global warming thresholds as seen in the UK earth system model. *Journal of Climate*, *35*(1), 29–48. https://doi.org/10.1175/JCLI-D-21-0234.1

Tilmes, S., Fasullo, J., Lamarque, J.-F., Marsh, D. R., Mills, M., Alterskjaer, K., et al. (2013). The hydrological impact of geoengineering in the geoengineering model intercomparison project (GeoMIP). *Journal of Geophysical Research: Atmospheres*, *118*(19), 11–036. https://doi.org/10.1002/jgrd.50868

Tilmes, S., Richter, J., Kravitz, B., MacMartin, D., Glanville, A., Visioni, D., et al. (2021). Sensitivity of total column ozone to stratospheric sulfur injection strategies. *Geophysical Research Letters*, *48*(19), e2021GL094058. https://doi.org/10.1029/2021GL094058

Tilmes, S., Richter, J. H., Kravitz, B., MacMartin, D. G., Mills, M. J., Simpson, I. R., et al. (2018a). CESM1 (WACCM) stratospheric aerosol geoengineering large ensemble project. *Bulletin of the American Meteorological Society*, *99*(11), 2361–2371. https://doi.org/10.1175/BAMS-D-17-0267.1

Tilmes, S., Richter, J. H., Mills, M. J., Kravitz, B., MacMartin, D. G., Garcia, R. R., et al. (2018b). Effects of different stratospheric SO_2 injection altitudes on stratospheric chemistry and dynamics. *Journal of Geophysical Research: Atmospheres*, *123*(9), 4654–4673. https://doi.org/10.1002/2017JD028146

Tilmes, S., Visioni, D., Jones, A., Haywood, J., Séférian, R., Nabat, P., et al. (2022). Stratospheric ozone response to sulfate aerosol and solar dimming climate interventions based on the G6 geoengineering model intercomparison project (GeoMIP) simulations. https://doi.org/10.5194/acp-22-4557-2022

Trenberth, K. E., & Dai, A. (2007). Effects of Mount Pinatubo volcanic eruption on the hydrological cycle as an analog of geoengineering. *Geophysical Research Letters*, *34*, L15702. https://doi.org/10.1029/2007GL030524

UNEP. (2021). *Emissions gap report 2021: The heat is on - A world of climate promised not yet delivered*. UN. [Book].

UNEP. (2023). One atmosphere: An independent expert review on solar radiation modification research and deployment. Retrieved from https://wedocs.unep.org/20.500.11822/41903

Vallis, G. K., Zurita-Gotor, P., Cairns, C., & Kidston, J. (2015). Response of the large-scale structure of the atmosphere to global warming. *Quarterly Journal of the Royal Meteorological Society*, *141*(690), 1479–1501. https://doi.org/10.1002/qj.2456

Visioni, D., Bednarz, E. M., Lee, W. R., Kravitz, B., Jones, A., Haywood, J. M., & MacMartin, D. G. (2023a). Climate response to off-equatorial stratospheric sulfur injections in three earth system models–Part 1: Experimental protocols and surface changes. *Atmospheric Chemistry and Physics*, *23*(1), 663–685. https://doi.org/10.5194/acp-23-663-2023

Visioni, D., Bednarz, E. M., MacMartin, D. G., Kravitz, B., & Goddard, P. B. (2023b). The choice of baseline period influences the assessments of the outcomes of stratospheric aerosol injection. *Earth's Future*, *11*(8), e2023EF003851. https://doi.org/10.1029/2023EF003851

Visioni, D., MacMartin, D. G., Kravitz, B., Boucher, O., Jones, A., Lurton, T., et al. (2021). Identifying the sources of uncertainty in climate model simulations of solar radiation modification with the G6sulfur and G6solar geoengineering model intercomparison project (GeoMIP) simulations. *Atmospheric Chemistry and Physics*, *21*(13), 10039–10063. https://doi.org/10.5194/acp-21-10039-2021

Visioni, D., MacMartin, D. G., Kravitz, B., Lee, W., Simpson, I. R., & Richter, J. H. (2020). Reduced poleward transport due to stratospheric heating under stratospheric aerosols geoengineering. *Geophysical Research Letters*, *47*(17), e2020GL089470. https://doi.org/10.1029/2020GL089470

Visioni, D., Pitari, G., Tuccella, P., & Curci, G. (2018). Sulfur deposition changes under sulfate geoengineering conditions: Quasi-biennial oscillation effects on the transport and lifetime of stratospheric aerosols. *Atmospheric Chemistry and Physics*, *18*(4), 2787–2808. https://doi.org/10.5194/acp-18-2787-2018

Visioni, D., Robock, A., Haywood, J., Henry, M., Tilmes, S., MacMartin, D. G., et al. (2023c). G6-1.5 K-SAI: A new Geoengineering Model Intercomparison Project (GeoMIP) experiment integrating recent advances in solar radiation modification studies. *EGUsphere*, *2023*, 1–21.

Waugh, D. W., Grise, K. M., Seviour, W. J., Davis, S. M., Davis, N., Adam, O., et al. (2018). Revisiting the relationship among metrics of tropical expansion. *Journal of Climate*, *31*(18), 7565–7581. https://doi.org/10.1175/JCLI-D-18-0108.1

Wells, A. F., Henry, M., & Bednarz, E. M. (2023). Code for "identifying climate impacts from different stratospheric aerosol injection strategies in UKESM1" [Code]. *Zenodo*. https://doi.org/10.5281/zenodo.10302916

Wells, A. F., Jones, A., & Dalvi, M. (2023). Data for "identifying climate impacts from different stratospheric aerosol injection strategies in UKESM1" [Dataset]. *Zenodo*. https://doi.org/10.5281/zenodo.10302574

Wells, A. F., Jones, A., Osborne, M., Damany-Pearce, L., Partridge, D. G., & Haywood, J. M. (2023). Including ash in UKESM1 model simulations of the Raikoke volcanic eruption reveals improved agreement with observations. *Atmospheric Chemistry and Physics*, *23*(7), 3985–4007. https://doi.org/10.5194/acp-23-3985-2023

Wheeler, T., & Von Braun, J. (2013). Climate change impacts on global food security. *Science*, *341*(6145), 508–513. https://doi.org/10.1126/science.1239402

Yool, A., Popova, E. E., & Anderson, T. R. (2013). Medusa-2.0: An intermediate complexity biogeochemical model of the marine carbon cycle for climate change and ocean acidification studies. *Geoscientific Model Development*, *6*(5), 1767–1811. https://doi.org/10.5194/gmd-6-1767-2013

Zhang, Y., MacMartin, D. G., Visioni, D., Bednarz, E. M., & Kravitz, B. (2024). Hemispherically symmetric strategies for stratospheric aerosol injection. *Earth System Dynamics*, *15*(2), 191–213. https://doi.org/10.5194/esd-15-191-2024

Zhao, M., Cao, L., Bala, G., & Duan, L. (2021). Climate response to latitudinal and altitudinal distribution of stratospheric sulfate aerosols. *Journal of Geophysical Research: Atmospheres*, *126*(24), e2021JD035379. https://doi.org/10.1029/2021JD035379